Simplified pumped thermal energy storage using a two-way Stirling cycle

Journal of Energy Storage 73 (2023) 108994

Contents lists available at ScienceDirect

Journal of Energy Storage

journal homepage: www.elsevier.com/locate/est

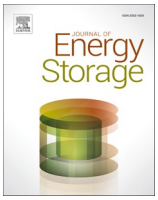

Research papers

Simplified pumped thermal energy storage using a two-way Stirling cycle

Martin Nilsson

Division of Fluid Mechanics, Department of Mechanics and Maritime Sciences, Chalmers University of Technology, SE-412 96 Göteborg, Sweden

ARTICLE INFO

Keywords:
Energy storage
Heat pump
Stirling engine
Pumped thermal energy storage
Thermal storage

ABSTRACT

The present work introduces a concept of pumped thermal energy storage based on the Stirling cycle. It provides a smaller sized energy storage and power conversion unit than what is typically proposed using pumped thermal energy storage systems, while offering high round-trip efficiencies despite a simple concept. Conventional systems are typically Brayton cycle based with two-tank liquid thermal storages on both the hot and the cold side. The proposed concept utilizes a single Stirling machine for both energy discharge and charge, and this is the first study where this approach is investigated. It is combined with a single-tank liquid thermal storage on the hot side and a fan and radiator combination on the cold side. Round-trip efficiencies for several storage fluids are analyzed using high-fidelity validated models, with relevant components and power losses. It is shown that round-trip efficiencies of up to 49 % at the generator are possible when using high-temperature fluids and with low-temperature synthetic fluids round-trip efficiencies of 32 % are obtained.

1. Introduction

In the years leading up to 2022 the world has seen climate and weather emergencies unprecedented in modern times. The droughts of 2022 in Europe, North America and China highlighted the effect on millions of people for such basic needs as drinking-water [1–3]. Most of these effects, especially their increased severity and frequency, are attributed to the release of greenhouse gases into the atmosphere since the dawn of the industrial revolution. The energy sector is responsible for almost three-quarters of the emissions that have already pushed global average temperatures 1.1°C higher than before the pre-industrial age [4]. It is widely understood the energy sector must be a central part of the solution and the International Energy Agency describes the future energy sector to be "more electrified, efficient, interconnected and clean."

In most markets renewable energy technologies such as solar photovoltaics and wind turbines are the new-build energy sources with lowest cost. Analysis by the International Energy Agency estimates their share of total electricity generation to be between 23% and 40% already in 2030 [4].

Since the dominant technologies available are variable and non-dispatchable, the transition to a power system with high degree of renewables is challenging. An increased share of variable renewable energy means a reduction in the relative energy buffer provided by the mechanical inertia of spinning generators, and it translates to less stability in the electric power system. The key to system stability is flexibility and dispatchability on both the generation and the demand side. Solutions to increase them include demand-side management through load shifting and consumption planning, behind-the-meter local energy storage, further expansion of grid interconnections, oversizing of variable renewable capacity and generation, and grid side energy storage.

Electro-chemical batteries, fly-wheels and capacitors are starting to emerge as a preferred solution for short duration storage and fast balancing but are currently not economically viable beyond four hours of duration [5]. For the longer term, pumped hydro-electric storage (PHES) is an established technology with high maturity and currently supplies circa 95% of global energy storage, but it cannot be significantly expanded due to geographical limitations [6]. Thermo-mechanical storage technologies (TMES) are, on the other hand, well suited to long duration energy storage at low cost and several technologies within this group are described in [5,7–10], such as pumped thermal energy storage (PTES), compressed air energy storage (CAES), Carnot batteries (CB), and liquid air energy storages (LAES). Power-to-gas-to-power technologies, e.g. using hydrogen (H_2), are also possible for long duration energy storage as mentioned in [5].

The purpose of this paper is to discuss a new development of thermo-mechanical energy storage based on the Stirling cycle. It is a variant of pumped thermal energy storage but suitable for smaller energy storages and smaller power sizes, while also allowing a conceptually simpler system with fewer components. It uses a Stirling cycle device for charging of the thermal storage and then utilizes that same equipment for the discharge process. It has a thermal storage on the hot side only,

E-mail address: martin@nidingen.com.

https://doi.org/10.1016/j.est.2023.108994
Received 29 June 2023; Received in revised form 5 September 2023; Accepted 10 September 2023
Available online 20 September 2023

Abbreviations

CAES	Compressed air energy storage
CB	Carnot battery
CHEST	Compressed heat energy storage
COP	Coefficient of performance
CSP	Concentrated solar power
DF	Discharge fraction
HTF	Heat transfer fluid
LAES	Liquid air energy storage
MVR	Mechanical vapor recompression
NTU	Number of transfer units
PCM	Phase change material
PHES	Pumped hydro-electric storage
PTES	Pumped thermal energy storage
RTE	Round-trip efficiency
TMES	Thermo-mechanical energy storage

Roman

cp	Specific heat [J/(kg•K)]
f	Frequency [Hz]
h	Enthalpy [J/kg]
m	Mass [kg]
$\dot{m}$	Mass flow [kg/s]
P	Pressure [Pa, bar]
pme	Pressure mean engine [bar]
s	Stroke [m]
t	Time [s]
P	Power [W]
Q, q	Heat flow [W]
T	Temperature [K,°C]
V	Volume [m^3, cm^3]
W	Work [W]

Greek

φ	Phase angle [°]
η	Efficiency [−]
ε	Effectiveness [−]
ρ	Mass density [kg/m^3]
ρ_E	Thermal energy density [kWh/m^3]
ρ_P	Power density [kW/m^3]

Subscripts

aux	Auxiliary
c	Cold
ch	Charge
dis	Discharge
h	Hot
init	Initial
loss	Loss from friction
mech	Mechanical
net	Including friction, mechanical or electric losses
swept	Swept by piston over the stroke
tank	Pertaining to storage tank
th	Thermodynamic, i.e. not including friction, mechanical or electric losses
working	Related to the working cycle

exchanging heat with the surroundings on the cold side. The proposed system is schematically described in Fig. 1.

It will first be investigated if it is possible to utilize a Stirling engine both as the heat pump and as the heat engine, i.e. to use one piece of equipment both for charging and discharging. Secondly, suitable types of storage, including choices of storage media, will be studied as will the eventual need of a thermal storage on the cold side. Thirdly, representative flows of energy and mass, temperature levels, and physical dimensions of the storage for a certain size of heat engine will be calculated. Ultimately an estimate of round-trip efficiency is made.

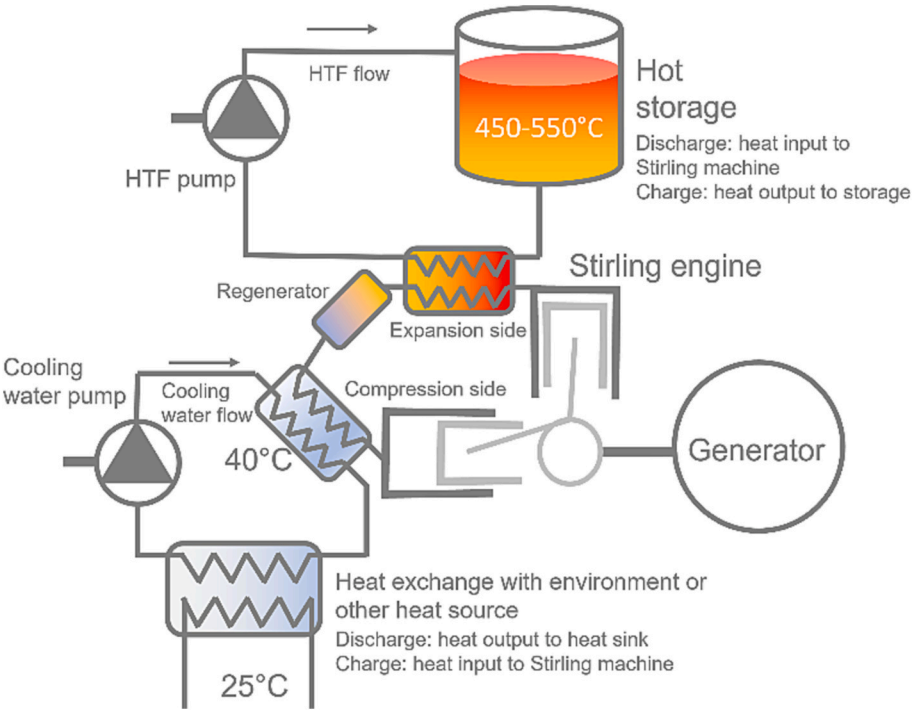

Fig. 1. A Stirling engine-based PTES with single tank hot storage heat exchanging with the environment on the cold side. Example temperatures using molten salt as storage and fluid medium and heat exchanging with the environment during a 25°C day. The Stirling machine charges the storage through a thermodynamic cycle while extracting heat from the surrounding environment, thereby augmenting the heat amount delivered to the storage. During system discharge the heat from the storage is used to power the Stirling engine, now acting as heat engine, and rejecting heat to the surroundings.

Finally, to assess the benefit of the heat pump during charging the proposed concept of pumped thermal storage (PTES) is compared to a, directly heated storage (Carnot battery) using the same storage type and dimensions, and the same heat engine.

Similar concepts based on the Stirling cycle have been presented [11–15], but these do not use a thermodynamic cycle for the charging, i.e. they are Carnot batteries, and do not extract heat from the surroundings during charging. The system developed by Azelio AB [11,12] is shown in Fig. 2. It uses a one tank storage with a phase change material and utilizes a Stirling cycle for the heat-to-power discharge. The storage is electrically heated during charge via a liquid heat transfer circuit, and a similar liquid circuit transports heat to the Stirling engine during system discharge. A similar type of system was presented in 2016 by Glatzmeier [13]. It used a latent thermal storage system coupled to a thermo-electric generator for converting thermal energy to electricity. A heat pipe transported heat from the storage to the generator. An updated concept using a Stirling engine to convert heat to electricity was described by Rea [14] in 2019. A related concept is proposed by Tetteh et al. [15] which couples a Stirling engine to an electrically heated sensible thermal storage with either a liquid or a solid. All four concepts are alike to what is proposed in the present paper, except that here the storage material, a fluid, circulates and also performs the function of the heat transfer fluid. The concepts by Azelio, Glatzmeier and Rae utilize a phase change material in the storage and transport the heat from the storage to the converter by a liquid metal heat pipe or pumped liquid metal circuit. In the concept by Tetteh et al. an internally placed heat conductor of unspecified design transports heat from a sensible storage to the Stirling engine.

In contrast to the electrically heated storages of Azelio, Glatzmeier, Rea, and Tetteh, thermodynamic cycles are used to charge pumped thermal energy storages. The choice of thermodynamic cycle is theoretically arbitrary, but a turbomachinery Brayton cycle is frequently used [16–20], since it can be operated in reverse, as both the heat pump and as the heat engine. Note the same turbomachinery cannot be used for charging (heat pump) and discharging (heat engine). Isentropic Ltd. proposed a storage system based on the Ericsson cycle [21]. An idealized Brayton-based PTES with one set of turbomachinery is shown in Fig. 3. Recuperated cycles are also used, as explained e.g. in [18], and in the setup shown in Fig. 3 the recuperator would be placed after the heat exchangers communicating with the storages, i.e. it would connect point 3 in the cycle with point 6.

It is worth noting that neither CB nor PTES system typically include any heat extraction from the surroundings during the charge process. Common PTES systems reject heat to the environment after charging (process step 3–4 in Fig. 3), but do not draw any heat from the surroundings. In the proposed concept, however, the surroundings act as heat source during charging. The energy input to the system is thus augmented by the heat drawn from the surroundings, thereby improving the round-trip-efficiency for this type of system beyond what would be possible in a Carnot battery configuration. During system discharge heat is rejected to the surroundings which then act as a heat sink.

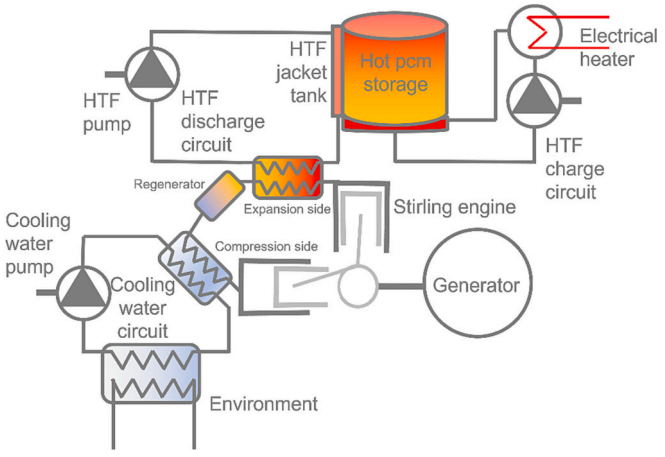

Fig. 2. Stirling cycle CB system with one-tank hot storage and the environment as heat sink. The electrical heater is run during charging only and is shut-off during discharging, during which the Stirling heat engine is used.

The compressed heat energy storage (CHEST) also draws heat from the surroundings during charge, as described in [16] and schematically shown in Fig. 4. The CHEST concept uses low-temperature heat from the environment to make steam which is compressed mechanically to increase its temperature, i.e. energy content, and the thermal energy is stored in an array of thermal storages past the condensation point. A conventional Rankine cycle is typically suggested as power cycle for the discharge process.

The overviews by Olympios et al. [10] and Dumont et al. [9] give detailed overviews of different technologies and provide a techno-economic comparison. Compared to established technologies, thermo-mechanical storage technologies have generally lower round-trip efficiencies, between 50% and 70%, but also low-cost energy storage and long lifespans, making them potentially interesting for the long-term storage of surpluses of renewable energy which would otherwise be curtailed. In most instances of thermal energy storage systems it is possible to decouple the energy storage capacity from the conversion power. Adding additional storage is in most cases only related to the physical size of the storage, leaving the conversion machinery unchanged. The marginal cost of adding additional thermal storage capacity is therefore often lower than competing technologies, e.g. electrochemical batteries, making them suitable for longer duration energy storage.

Furthermore, the reviews in references [5, 7–10] show most technology development in this area to be centered on higher power systems, with some starting at 1 MW of discharge power while most seem to aim for a few 10's to several 100's of MW of discharge power. No technology is specifically mentioned in the context of smaller systems less than a few 100's of kW's, although some of them are theoretically usable in smaller sizes.

Energy densities are stated in [10] as 3–20 kWh/m^3 for CAES, 20–50 kWh/m^3 for Brayton-based PTES and 40–100 kWh/m^3 for CHEST. Power densities are listed as 0.5–2 kW/m^3 for CAES, 1–15 kW/m^3 for Brayton-based PTES and 0.5–17 kW/m^3 for CHEST. Energy or power densities for Carnot batteries are not given but are expected to be similar to Brayton PTES.

The proposed concept enables a smaller thermal energy storage, in both capacity and power rating, and with less complexity than offered by many other technologies, e.g. conventional PTES systems based on the Brayton cycle with two sets of turbomachinery. Energy and power densities for the proposed concept will be calculated and compared to the other technology types.

2. Method of assessment

In the context of this paper thermal energy storage systems are systems where electricity is converted to thermal energy, stored in the thermal energy storage(s) and, at time of demand, converted back to electricity. Their most important metric is the round-trip efficiency (RTE), defined as the ratio between energy input and energy output over a complete charge-discharge cycle. A theoretical and reversible system would yield an RTE of 100%, but with realistic component efficiencies and heat losses RTE is typically 30–70%, depending on the temperatures available in the heat source and sink, respectively.

Different configurations of the proposed concept are modeled as transient system models containing relevant components, each modeled

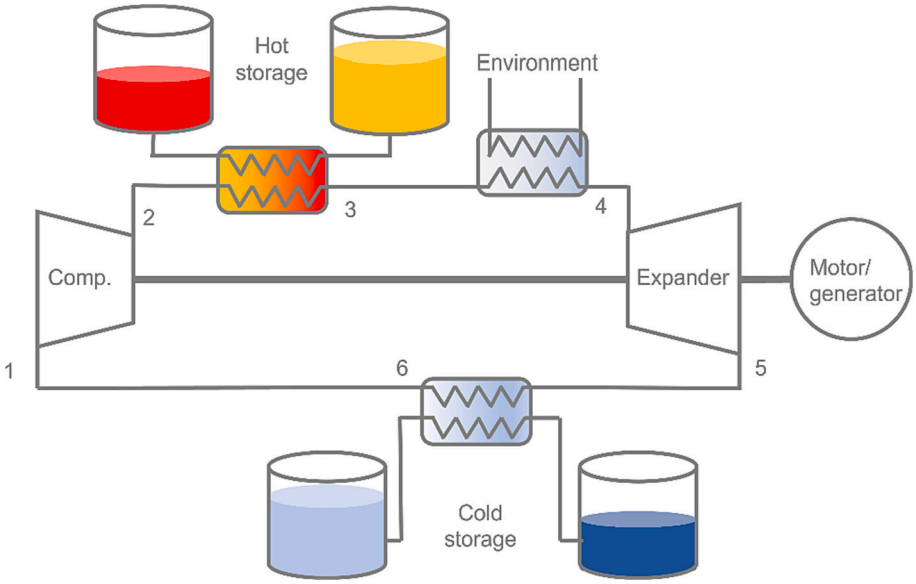

Fig. 3. Brayton cycle PTES system with two-tank storages and without. During system charging, the working fluid flows clockwise (1–2–3-4-5-6), while it flows counter-clockwise during system discharge. Note, in reality the charge and discharge processes require two sets of turbomachinery, while the heat exchangers and storages remain the same.

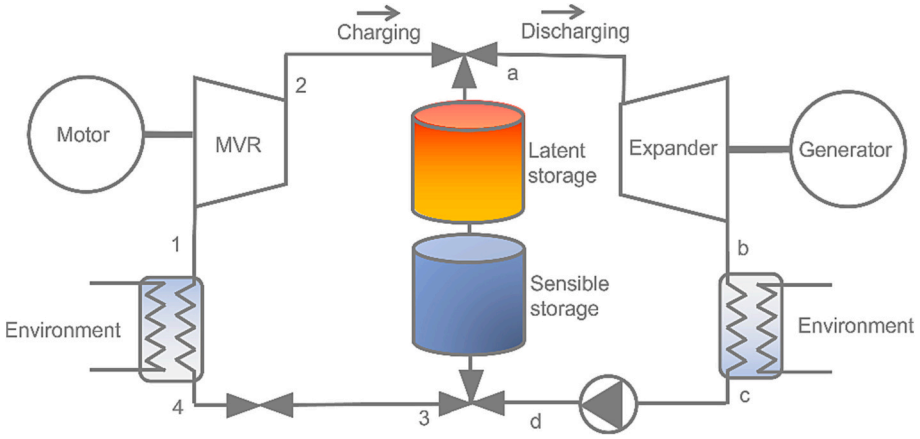

Fig. 4. CHEST system with water as working media, mechanical vapor recompression for charging and a Rankine cycle for discharge. In the charge process water evaporates sub-atmospherically using heat from the surroundings (4–1). The resulting steam is compressed and heated using mechanical vapor recompression (1–2). The hot steam charges a latent thermal storage while condensing and is next sub-cooled in a sensible thermal storage (2–3), before being expanded (3–4) and the process starts over. The discharge process is quite similar to many concentrated solar power (CSP) plants and is a standard Rankine process where steam is generated by the heat stored in the thermal storage (d-a) and expanded (a-b) to provide mechanical, and thus electrical energy, before being condensed (b-c) and circulated via a feed-water pump (c-d) for the process to start over.

with the relevant physics.[1] The models consist of components representing a Stirling engine and Stirling heat pump, liquid circuits for the transport of heat to and from the heat source and sink, thermal energy storage, a fan, a heat exchanger, an electric motor, and a generator. Component models are built and validated against experimental data where available or, for off-the-shelf components, created using manufacturer's data. The complete system model has not been validated against experimental data for a complete system given that none exist due to the conceptual state of the proposal. However, where possible individual components are validated against test data.

For each configuration results are extracted and compared to each other. Round-trip efficiency, flows of energy and heat, temperature levels, discharge efficiency are examples of data points used to represent the performance of each configuration.

One configuration of the pumped Stirling energy storage is compared to a Stirling based Carnot battery to determine the effect of the heat pump action of the Stirling engine on the round-trip efficiency. The method used for comparison is numerical simulation of the systems of interest and direct comparison of key metrics, e.g. round-trip efficiency, storage volume, average discharge power and discharged energy. Finally, values for round-trip efficiency are compared to data from literature for conventional turbomachinery-based PTES systems.

2.1. Stirling engine

The Stirling engine is modeled using a transient quasi-1D finite volume code created and validated for Stirling engines. A detailed description of the code is found in [23] while the engine concept is presented in [12]. The code is used to model the thermodynamics of the working gas channel over a large operational envelope of boundary temperatures, cycle frequencies, cycle average pressures, piston swept volumes, and expansion-to-compression phase angles. The operational envelope for the present work is tabulated in Table 1.

In the table, T_h is the hot side cycle average temperature, T_c is the cold side cycle average temperature, φ is the expansion to compression phase angle, V_{swept} is swept volume in the working cylinders, f is piston frequency, and pme is average cycle pressure. Data from the simulation code at each operational point is extracted and used to create a meta-

[1] Built in the Modelica [22] language using Wolfram SystemModeler version 13.1

Table 1
Operational envelope for a Stirling heat engine.

	Min	Max	Unit
T_h	550	900	K
T_c	293	333	K
φ	90	120	°
V_{swept}	145	290	cm^3
f	15	25	Hz
pme	100	150	bar

model of the final design using multi-variable linear regression fitted to the data using the least-squares method. The meta-model takes as input the operational parameters and outputs thermodynamic work, heat input and heat output so that:

$$Q_{hot} = f_1(f, pme, V, \varphi, T_h, T_c) \quad (1)$$

$$Q_{cold} = f_2(f, pme, V, \varphi, T_h, T_c) \quad (2)$$

$$W_{th} = f_3(f, pme, V, \varphi, T_h, T_c) \quad (3)$$

for each of the two processes charge and discharge. Q_{hot} is the heat exchange with the hot side, Q_{cold} is the heat exchange with the cold side, and W_{th} is the pressure-volume work performed by the working gas on the pistons. The functions f_1 and f_2 have the same expression but different coefficient values C, while f_3 is slightly different. The mean and maximum errors for each are shown in Table 2. The function f_1 and f_2 is:

$$\begin{aligned} f_1 = f_2 &= C_0 + C_1\cdot T_h + C_2\cdot T_c + C_3\cdot V + C_4\cdot\varphi + C_5\cdot f + C_6\cdot pme + C_7\cdot V\cdot f \\ &+ C_8\cdot V\cdot pme + C_9\cdot V\cdot T_h + C_{10}\cdot V\cdot\varphi + C_{11}\cdot V\cdot T_c + C_{12}\cdot f\cdot pme + C_{13}\cdot T_h\cdot f \\ &+ C_{14}\cdot T_h\cdot pme + C_{15}\cdot\varphi\cdot f + C_{16}\cdot\varphi\cdot pme + C_{17}\cdot V\cdot f\cdot pme + C_{18}\cdot T_h\cdot V\cdot p \\ &+ C_{19}\cdot T_h\cdot V\cdot f + C_{20}\cdot V\cdot\varphi\cdot p + C_{21}\cdot V\cdot\varphi\cdot f + C_{22}\cdot f^2 + C_{23}\cdot f^2\cdot pme + C_{24}\cdot V^2 \\ &+ C_{25}\cdot Tc\cdot V\cdot f + C_{26}\cdot T_c\cdot V\cdot pme + C_{27}\cdot T_c\cdot f + C_{28}\cdot T_c\cdot pme + C_{29}\cdot Th^2 \\ &+ C_{30}\cdot T_h\cdot V\cdot pme + C_{31}\cdot T_h\cdot f\cdot pme + C_{32}\cdot T_h\cdot\varphi \end{aligned} \quad (4)$$

The expression for f_3 is:

$$\begin{aligned} f_3 &= C_0 + C_1\cdot T_h + C_2\cdot T_c + C_3\cdot V + C_4\cdot\varphi + C_5\cdot f + C_6\cdot pme + C_7\cdot V\cdot f \\ &+ C_8\cdot V\cdot pme + C_9\cdot V\cdot T_h + C_{10}\cdot V\cdot T_c + C_{11}\cdot f\cdot pme + C_{14}\cdot T_h\cdot f \\ &+ C_{15}\cdot T_h\cdot pme + C_{16}\cdot T_h\cdot V\cdot pme + C_{17}\cdot T_h\cdot V\cdot f + C_{18}\cdot f^2 + C_{19}\cdot V^2 \\ &+ C_{20}\cdot Tc\cdot V\cdot f + C_{21}\cdot T_c\cdot f + C_{22}\cdot T_c\cdot pme + C_{23}\cdot Th^2 + C_{24}\cdot T_h\cdot f\cdot pme \\ &+ C_{25}\cdot T_h\cdot V\cdot\varphi + C_{26}\cdot T_h\cdot\varphi + C_{27}\cdot Th^2\cdot V + C_{28}\cdot V^2\cdot Th \end{aligned} \quad (5)$$

The coefficients for the discharge process for models f_1, f_2 and f_3 are given in Appendix A.

The meta-model is inserted into the systems model for later simulation as a complete system.

Losses from internal friction and mechanical auxiliaries are represented by an empirical model built on data from bench testing of a Stirling engine of relevant size but lower technological level regarding the mechanical design [24]. It is adjusted to represent a new development with lower friction. The losses depend primarily on frequency, f, and average cycle pressure, pme, with a small influence from the cold side temperature, T_c. A representation of loss can be written:

$$\begin{aligned} W_{loss} &= f_4(f, pme, T_c) \\ &= C_0 + C_1\cdot f + C_2\cdot pme + C_3\cdot T_c + \ldots C_4\cdot f\cdot pme + C_5\cdot f\cdot pme\cdot T_c + C_6\cdot f^2 \end{aligned} \quad (6)$$

The mechanical work output, W_{mech}, from or input to the machine is calculated as.

$$W_{mech} = W_{th} + W_{loss} \quad (7)$$

Table 2
Meta-model data fit.

	mean [%]	abs(max) [W]
$Q_{hot,charge}$	3.3	1390
$Q_{cold,charge}$	2.1	440
$W_{th,charge}$	2.3	1300
$Q_{hot,discharge}$	1.5	740
$Q_{cold,discharge}$	2.3	830
$W_{th,discharge}$	3.8	780

2.2. Electric motor-generator

The motor-generator is conceptually a single device, but for the sake of simplicity in modelling it is built as two discrete components. The motor-generator is assumed to be a synchronous permanent magnet device in efficiency class IE3 for electric motors when functioning as motor and with the same efficiency when acting as generator. The design efficiency is assumed constant at 95%, which is on the conservative side when comparing to [19] which assumes 98% electric efficiency for the motor-generator. The electric power output and input are thus:

$$P_{generator} = 0.95\cdot W_{mech} \text{ for discharge} \quad (8)$$

$$P_{motor} = W_{mech}/0.95 \text{ for charge} \quad (9)$$

2.3. Thermal storages

Recirculated one-tank thermal storages are represented by a serial array (vector) of lumped volume models with quasi-static mass balance and dynamic energy balance. No additional axial mixing or axial heat transfer is included beyond what occurs implicitly due to the number of discrete volumes being finite. All recirculated storages modeled in this paper have sixteen discrete volume elements, a balance between model speed and spatial resolution. The defining equations in each volume element are mass balance and energy balance:

$$\dot{m}_{in} + \dot{m}_{out} = 0 \quad (10)$$

$$\dot{m}_{in}\cdot h_{in} + \dot{m}_{out}\cdot h_{out} + Q = m\cdot c_p\cdot\frac{dT}{dt} \quad (11)$$

with m as mass, ṁ as mass flow, h as enthalpy, Q as heat flow, c_p as specific heat, T as temperature and t as time. If Q is zero, the volume does not exchange heat with the surroundings and is adiabatic. In the present work the storages are considered perfectly insulated. Given the modular nature of the model, adding this at a later stage is quite straightforward.

2.4. Fan and radiator

A fan and radiator heat exchanger are used to exchange heat in the cold end of the system. The fan is a 630 mm axial fan. The radiator is 725 mm wide, 805 mm high and has a thickness of 52 mm. It has 144 channels for the coolant mixture that are externally finned at just below 2 mm pitch for increased air-to-radiator heat transfer. The gas side pressure loss is 117 Pa with an air flow of 7000 m^3/h and 25°C. A correlation for its heat transfer effectiveness is built from test data.

$$\varepsilon = 0.389979\cdot ln(\text{NTU}) + 0.508271 \quad (12)$$

The fan model is a 0D-model of a generic fan built from the manufacturer's fan curves [25]. The nominal fan air flow as a function of its nominal pressure increase is tabulated and the model interpolates in the table to find the pressure increase which is numerically matched to the pressure drop over the heat exchanger. The model converges to the correct air flow after a few iterations.

From the known mass flows the effectiveness is calculated using Eq. (12), and the heat flow q is calculated through.

$$q_{max,air} = \dot{m}_{air} \cdot c_p \cdot \left(T_{liquid,in} - T_{air,in}\right) \quad (13)$$

$$q_{max,liquid} = \dot{m}_{liquid} \cdot c_p \cdot \left(T_{liquid,in} - T_{air,in}\right) \quad (14)$$

$$q_{max} = max\left(q_{max,air}; q_{max,liquid}\right) \quad (15)$$

$$q = q_{max} \cdot \varepsilon \quad (16)$$

In steady-state operation the fan is estimated to draw about 450 W. During cycle studies, the fan model calculates the power consumption from the fan affinity laws and includes this in the auxiliary power consumption.

2.5. Auxiliaries

The complete system has auxiliary sub-systems and components which consume power. Examples include the cold side liquid pump, the pump for the heat transfer fluid on the hot side, and the electronic control unit for the control of the system. For the purpose of this study each of these powers is assumed to be constant. Based on hand-calculations and supplier's data they are estimated to 350 W and are assumed constant throughout the cycle.

2.6. Fluid properties

Multiple fluids are used in the system model: coolant, air, storage medium and heat transfer fluids. In the proposed concept the storage medium is the same as the heat transfer fluid. None of the fluids used in this study, is available in the Modelica Standard Library [22], with the exception of air, and temperature dependent expressions are needed to create the necessary media models. Properties for water-glycol mixtures are obtained from [26] as temperature and concentration dependent equations; temperature dependent properties for Sodium (Na) are taken from Fink and Leibowitz [27]; molten salt and synthetic thermal storage fluid properties are obtained from the respective manufacturer. The data for the latter include the variation of density, specific heat capacity, thermal conductivity, and viscosity with temperature in table form and each property is curve fitted to obtain polynomial equations with temperature as the independent variable. All water glycol-mixtures are modeled as 50% concentration by volume. A brief discussion of the properties of possible heat transfer fluids is included in Section 3.2.

3. Description of the proposed concept

The proposed system for pumped thermal storage was briefly described previously, it is shown in Fig. 1. It consists of one Stirling engine for heat to work conversion during discharge and work to heat conversion during charge. During discharge, heat from the storage is converted in the Stirling engine to mechanical shaft work, which can be used to drive a generator. The residual heat is rejected to the environment or put to use in a constant temperature heat sink. In the charge phase the reverse Stirling cycle pumps heat from the environment to the hot storage. Heat is here drawn from the environment or a suitable constant temperature heat source, which could be utilized for cooling purposes. The hot storage is a liquid sensible storage in a one-tank configuration, and on the cold side the system heat exchanges with the environment. Liquid circuits are used to transfer heat to and from the Stirling unit. On the cold side the fluid is suitably a water-glycol brine, whereas on the hot side a high temperature fluid (HTF) is needed. The HTF can double as storage medium in the sensible storage for added simplicity and reduced part count. Going forward, the nominal tank volume will be 15 m^3, the ambient temperature will be 25°C, a radiator and fan combination will be used to exchange heat with the low temperature source/sink, and the mass flow of heat transfer fluid will be set to 1.5 kg/s, for all fluids.

3.1. Stirling engine

A Stirling engine for the proposed application needs to both accept heat from and reject heat to liquid circuits. It needs to be conceptually similar to the engine presented in [12] which was adapted to accept heat from liquid Sodium, acting as heat transfer fluid, and designed for Hydrogen (H_2) as working gas. It furthermore rejected heat to the surroundings via a water-glycol circuit and a fan-radiator combination.

The present work retains some basic properties of that engine, but the working gas channel is re-designed for Helium (He) as working gas. Moreover it is envisioned that the mechanical arrangement now has lower mechanical losses than the aforementioned engine, and it is assumed mechanical friction and other mechanical losses are about half that of the engine discussed in [24]. This is a realistic assumption for a new development with state-of-the-art technologies such as electronically controlled pistons allowing seamless adjustment of piston stroke and expansion-to-compression phase angle. Note that a Stirling cycle device works on a closed cycle and exchanges heat with external sources and sinks through heat exchangers and can thus use un-pressured fluid circuits and storages, which enables substantial material savings over pressurized ones.

In the present work, the word ‘engine’ is used to also mean ‘device’ in some instances. Formally, an ‘engine’ is a device providing mechanical work, and when heat is the desired outcome, ‘heat pump’ is the preferred term. To avoid cluttering and repetition, the word ‘engine’ is here sometimes used to represent ‘engine and heat pump’ when Stirling based machinery is discussed. Context will make it clear if heat pump operation is also implied.

The re-design of the working gas channel is made using the previously transient quasi-1D finite volume code [23] as primary analysis tool, which is extensively validated against data from bench tests of relevant Stirling engines [12,23]. The main challenge is to design a gas channel that works well both as a heat engine and as a heat pump. Geometrical details of the gas channel of the final design are given in Table 3. The engine delivers 23 kW of discharge power at the generator with boundary temperatures of 873 K and 318 K and running at a frequency of 25 Hz, a stroke equivalent to 290 cm^3 of swept volume per cylinder, 150 bars of mean working pressure and an expansion-to-compression phase angle of -105°.

Using a Stirling engine as heat engine is well known to the author and was e.g. studied in [12,23,28]. It is also the most common use of the Stirling engine, discussed e.g. in [29,30]. The Stirling engine as heat pump in the current application is less well known and thermodynamic studies are made to investigate its behavior. The studies are initially made at constant operating conditions (temperatures, speed, mean working pressure and piston stroke) and several boundary temperatures are applied to investigate the performance with different source and sink temperatures. For each cold (source) temperature, several hot (sink) temperatures are applied for a total of 28 cases, see Fig. 5. The important metric is the coefficient of performance, which is defined as the ratio between delivered heat and, in this case, thermodynamic work input, so that:

$$COP_{th} = Q_h / W_{th} \quad (17a)$$

Note the work input could also be selected at some other system boundary to provide a coefficient of performance based on the mechanical power input (shaft work) or electrical power input to the motor.

Table 3
Some geometrical data on the Stirling engine.

Parameter	Value	Unit
Heat exchanger external area, hot side	0.410	m^2
Heat exchanger external area, cold side	0.437	m^2
Swept volume, expansion side	290.0	cm^3
Swept volume, compression side	290.0	cm^3

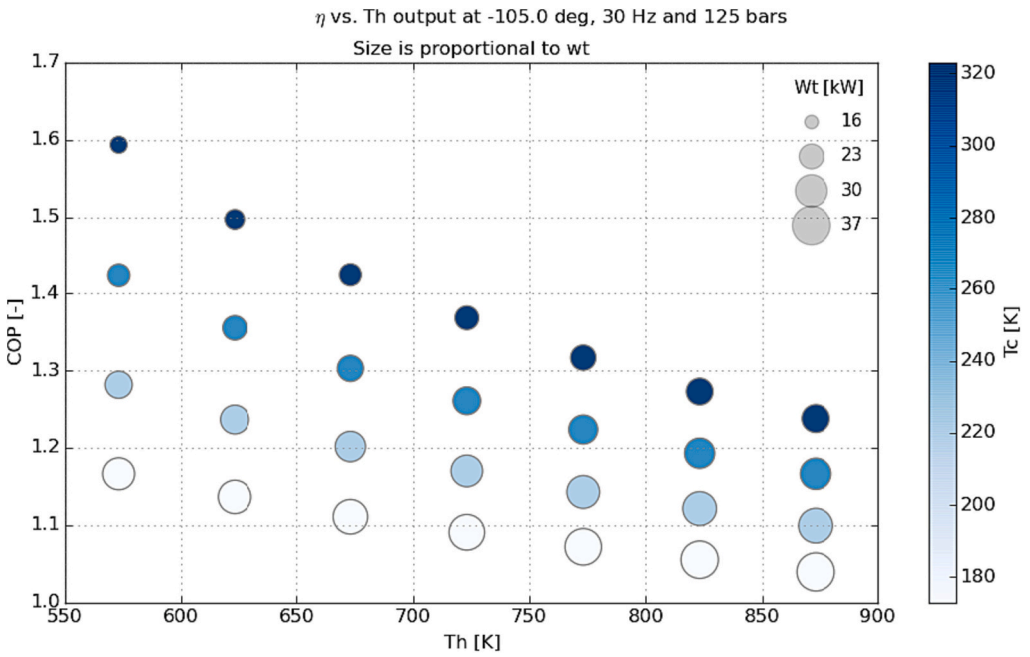

Fig. 5. COP_{th} as a function of temperatures T_c and T_h. Shaft speed 30 Hz, phase angle 105°, mean working pressure 125 bars and swept volume 290 mm^3. Not including friction and auxiliaries, generator efficiency or parasitic losses. Marker size is proportional to pressure-volume work input.

In the present section the definition of COP according to Eq. (17a) is used.

The studies show the gas channel to perform well as heat pump. As all heat pumps it reaches higher coefficients of performance (COP) at larger ratios T_c/T_h and lower temperature lifts $T_h - T_c$. For example, with 323 K on the cold end it achieves a COP_{th} of 1.24 with a higher hot end temperature of 873 K and almost 1.6 with a lower hot end temperature of 573 K. A realistic charging phase using liquid Sodium as storage fluid will start at 500°C on the hot side and a COP of 1.31 and finish at 600°C with a COP of 1.24. Using synthetic oil and charging between, say, 325°C and 400°C, COP starts at 1.55 and falls to 1.42 at the end of charge.

Furthermore, it is noted that the Stirling cycle is relatively insensitive to boundary temperatures T_c and T_h in that it can pump heat effectively over a surprisingly large temperature difference. This is a consequence of the gas channel's insensitivity to boundary temperatures. When the temperature ratio T_c/T_h is large, COP is low and at some ratio T_c/T_h the COP will approach unity. When this happens, an electrical heater could be preferred instead of the Stirling heat pump. Note that the point at which this happens does not only depend on the thermodynamics of the Stirling heat pump, but also on its mechanical and electrical losses, and the operating cost of the Stirling device and the electrical heater.

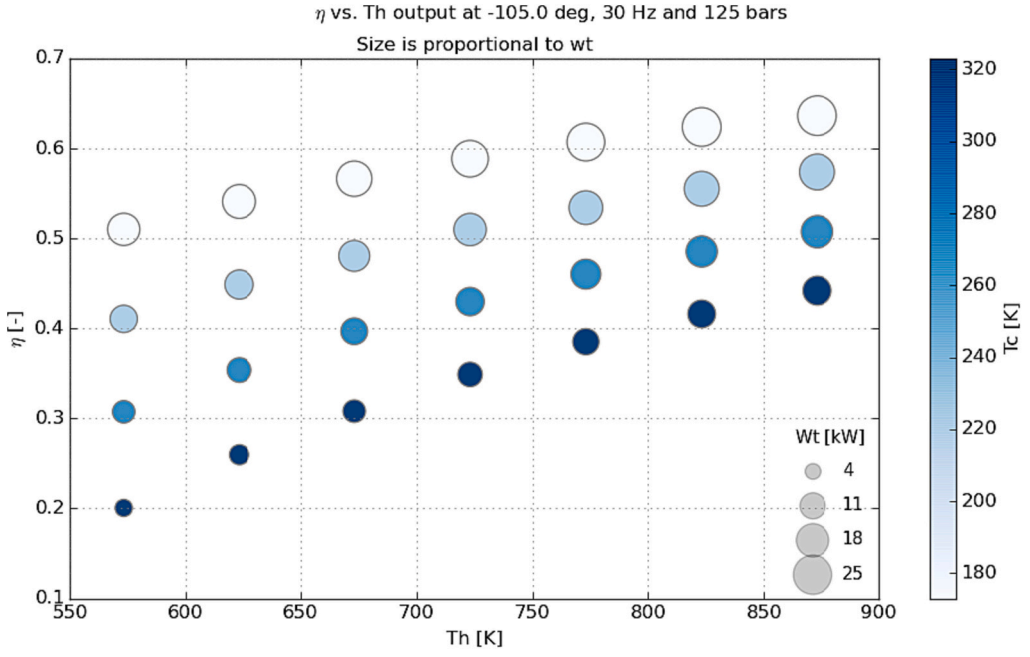

Fig. 6. η_{th} as a function of temperatures T_c and T_h. Shaft speed 30 Hz, phase angle -105°, mean working pressure 125 bars and stroke 80 mm. Not including friction and auxiliaries, generator efficiency or parasitic losses. Marker size is proportional to work output.

The efficiencies of the discharge process are estimated in the same manner as for the charge process, see Eq. (17b).

$$\eta_{th} = W_{th}/Q_h \quad (17b)$$

A thermodynamic efficiency of 0.44 is reached when the boundary temperatures are 873 K and 323 K, see Fig. 6. Likewise, from the same figure the discharge efficiency is estimated to be 0.20 for a hot end temperature close to 573 K and a cold end temperature of 323 K.

A realistic discharging phase using liquid Sodium as storage fluid starts with the hot end temperature at 600°C and an efficiency of 0.44 and finishes at 500°C with an efficiency of 0.39. Using synthetic oil and discharging between 400°C and 325°C, the efficiency becomes 0.31 at the beginning of discharge and falls to 0.23 at the end.

The figure of merit for the combined charge-discharge cycle is the round-trip efficiency, RTE, which for a thermal storage system is defined as.

$$RTE = E_{dis}/E_{ch} \quad (18)$$

where E is energy. For steady state operation this can be re-written as.

$$RTE = P_{dis}/P_{ch} = \eta \cdot COP \quad (19)$$

where P is power. The thermodynamic round-trip efficiency RTE_{th} is calculated as 1.24·0.44 = 0.55 at 600°C and 1.42·0.31 = 0.44 at 400°C, with values for η and COP estimated from Figs. 5 and 6. A higher hot end temperature for a fixed cold end temperature results in a higher thermodynamic round-trip efficiency since the discharge efficiency increases more than the decrease in COP. However, it is necessary to include mechanical losses and the varying temperature in the storage over a full cycle for a complete assessment of RTE. The data in Figs. 5 and 6 are therefore only indicative in this regard.

A final note on the operation of a Stirling device. A Stirling engine is a closed cycle device, and its operating power can be controlled by means of varying the mass of working gas in the engine. This is often the preferred way of power control in Stirling engines, for example employed in the Solo V-160 and United Stirling V4X engines [31,32]. It allows the Stirling engine to operate over a wide range of power ratings for both discharge and charge while maintaining high efficiency. Olympios [10] discusses similar possibilities for power control with maintained efficiency and pressure ratio, central in Brayton cycles, in closed cycle Brayton devices under the moniker 'inventory control.' This means of control has been used in Stirling devices for decades.

3.2. Heat transfer fluid

There are several fluids available as heat transfer fluid or storage medium, or both. The choice of fluid to a large extent defines the operating temperatures of the cycle, greatly influencing the round-trip efficiency, and to a lesser extent defining the energy density. The maximum operating temperature of a fluid is usually defined by thermal stability or phase change and influences the material choice in heat exchangers, piping, and storage vessels. The minimum operating temperature can, for example, be defined by freezing or high viscosity. In the lower end of the operating range heat tracing might be required for some fluids or pumping power might be high.

Common fluids for thermal storage systems are mineral oil, synthetic oil, nitrate molten salt, chloride molten salt and Sodium. Some basic properties for these fluids are summarized in Table 4.

Of the fluid types listed above mineral oils have too low maximum temperature to be of interest, and chloride salts require material development to prevent corrosion. They are therefore excluded from the present study. Nitrate molten salts have maximum temperatures above 500°C and have high densities compared to synthetic oils and Sodium. In the case of a sensible and liquid thermal storage where the mass of the storage medium is a relevant parameter, nitrate salts require a smaller tank volume than the other two fluids for the same storage capacity.

Table 4
Properties for several fluids. Data from [16] and [23].

Type	Temperature range	Specific heat c_p	Density ρ
	°C	kJ/kg·K	kg/m^3
Mineral oil	10–300	2.37	775
Synthetic oil	10–400	2.37	886
Nitrate salt	230–565	1.51	1840
Chloride salt	450–850	1.03	1460
Sodium	99–800	1.30	830

When the storage volume is fixed, specific heat by volume, the product $\rho \cdot c_p$ [J/(m^3·K)], is a relevant parameter. Synthetic oil, nitrate salt and Sodium have volumetric specific heats of 2100, 2780 and 1080 kJ/(m^3·K), respectively and nitrate molten salt provides a higher storage capacity than either synthetic oil or Sodium for the same tank volume.

Sodium is stable up to 800°C and enables a high round-trip efficiency. It will, however, require nickel alloys in piping and heat exchangers in the hot parts of the system. In the current work, the maximum temperature is set to 600°C and systems discussed here permit the use of high-end stainless steels, for example Sandvik 253MA, an austenitic chromium-nickel steel with high creep strength, and avoid expensive nickel alloys.

Synthetic oil has the lowest maximum temperature of the three fluids and delivers the lowest round-trip efficiencies. The advantage of a lower maximum temperature, however, is that it permits cheap carbon steels or lower grade stainless steels in piping, heat exchangers and storage vessels, lowering component cost. It has a low viscosity at low temperatures and can be used without heat tracing and offers simple handling if the system needs to go down in temperature, e.g. during service.

Further studies on the system level will include synthetic oil, nitrate salt and Sodium. More specifically the synthetic oil and the nitrate salt to be studied are Omnisol and Omnistore MS-600 from Global Group.[2] The system performance for each fluid will be analyzed, with temperature limits defined according to the properties of each fluid. Maximum temperatures for each HTF (Sodium, Omnistore MS-600 and Omnisol) are in this study set to 600°C, 550°C and 400°C, respectively.

3.3. Hot side

The hot side of the system includes the thermal storage where thermal energy is stored sensibly or latently by raising the temperature of the storage medium. In the former case the storage medium is usually a liquid stored in a tank. In the latter case the storage medium is enclosed in a tank and undergoes a phase change during which it is mostly isothermal. Packed beds of solid material are possible as sensible storages but typically require a gas as heat transfer fluid and are not part of the scope for the present work, which assumes liquid heat transfer fluids.

3.3.1. Latent storage

One advantage of latent thermal storages is the stable temperature obtained during discharge, resulting in high efficiency throughout the discharge phase. A disadvantage is that it requires a separate heat transfer fluid to transfer heat to and from the storage to the heat engine. A latent heat thermal storage is not completely isothermal due to the finite thermal conductivities of the liquid and solid phases. In addition, melting or solidifying of actual alloy compositions do not occur at a single temperature but over a temperature interval. The result is a stable but slowly decreasing inlet temperature to the heat engine.

In the latent storages in development, aluminium-silica, AlSi, seems to be the most commonly used storage material, used for example in [18]. AlSi requires the use of corrosion protection to protect storage

[2] Thanks to Global Group for detailed fluid property tables

tanks from the corrosive properties of aluminium at high temperature. A possible solution is a ceramic coating applied via thermal spraying.

AlSi has a eutectic melting point of 577°C and in practice this will mean maximum operating temperatures close to 600°C over a large part of the operating cycle since temperature differences between the storage medium and the required heat transfer fluid must be considered. This means discharge efficiency will be high, but the charging COP will be compromised.

3.3.2. Sensible storage

The combination of a power cycle with a working gas and a liquid as the medium in a sensible storage requires indirect heat transfer via a heat exchanger from the power cycle. In the case of Stirling engines, this is always the case since all practical embodiments of the cycle built to date include a closed working space with a working gas in oscillating flow. On the other hand, as a consequence the storage tank can be unpressurized which reduces the cost of the tank. Moreover, liquids have in general more limited operating temperature ranges than pcm's and solids and also higher capital costs.

A sensible storage in the form of a solid thermocline is possible but is likely limited in heat transfer from the heat transfer fluid to the solid or within the solid itself owing to the limited thermal conduction of available materials such as concrete or aluminium. Moreover, due to the nature of solid thermoclines, the storage system must be oversized to achieve the required storage capacity or need to be supplemented by pcm's at the outlet. Olympios [10] mentions the possibility of segmenting the solid thermocline to stabilize the outlet temperature from the storage.

The fluid medium for a sensible liquid storage can double as heat transfer fluid so that the fluid circuit and the storage tank need not be separate vessels. The most common setup is the two-tank approach where double tanks are used on the hot side as displayed in in Fig. 3. A tank model is created in the systems model, Fig. 7, and a two-tank storage filled with Sodium is evaluated with the Stirling engine during system discharge. This model uses the environment as heat sink. The results show the inlet temperature to the heat exchanger is constant throughout discharge, allowing the engine to deliver at constant efficiency.

In the model, the Stirling engine mentioned in Section 3.1 will deliver 16 kW of shaft work and draw 45 kW from the hot storage with a heat source temperature of 860 K (representative of Sodium). The temperature drop across the hot heat exchanger is 22 K and for the discharge phase to last 14.4 h (60 % of 24 h) a tank volume of 78 m^3 is needed for each tank. The combined tank setup is thus extremely large, and likely very costly.

In a Stirling engine, the temperature drop over the hot heat exchanger is much lower than what can be achieved in e.g. a counter-flow heat exchanger in a Brayton cycle gas turbine. This is due to the oscillatory motion of the working gas in a Stirling engine causing its heat exchangers to be of the cross-flow type. Counter-flow heat exchangers with large temperature drops are not possible in Stirling engines.

One path to reducing the tank volume is to decrease the mass flow of the heat transfer fluid, but doing so lowers the average heat exchanger temperature, lowering engine output. A 50% reduction in mass flow means 500 W lower power output from the Stirling engine mentioned above, but it does on the other hand mean tanks only half as large as before. Another solution could be to place several Stirling engines in series to obtain a larger overall temperature drop, but it will result in low average temperature over the engine array. It also goes against the idea of this paper, which is to investigate a simpler system.

An alternative solution is a single storage tank with a temperature gradient like a thermocline, Fig. 8. In such a setup the storage medium is circulated back to the tank after passing the Stirling engine's heat exchanger. The temperature of the tank is thus successively lowered, but the decrease in heat exchanger inlet temperature is slower due to the presence of the temperature gradient. A one-tank thermocline storage on the hot side will over the duration of a discharge cycle deliver a slowly decreasing inlet temperature while the storage volume can be greatly reduced relative to a double tank setup. The temperatures delivered to the Stirling engine from a one-tank storage are expected to decrease almost linearly with time.

Due to the decreasing inlet temperature the Stirling engine will not operate at constantly high efficiency but will experience a reduction during the discharge phase. On the other hand, the COP will be higher at the beginning of the charge phase for the same reason. On the upside, the tank volume needed is much smaller than in a double tank storage. For Sodium, a volume of about 15 m^3 is needed to discharge the system over 14.4 h with sufficiently high inlet temperature (780 K) at end of discharge. It is significantly smaller than the 2·78 = 156 m^3 estimated for a double tank storage. Therefore, a single tank storage is preferred in the remainder of the work.

3.4. Cold storage or sink

The cold storage is where thermal energy is stored sensibly or latently by lowering the temperature of the storage medium. The initial studies made on the Stirling engine indicated a cold storage would not improve RTE compared to heat exchanging with the environment. The reason is that COP decreases while η increases with decreasing temperature ratio T_L/T_H, see for example Fig. 5. Cold storages are typically used in PTES systems based on the Brayton cycle where there is a need to

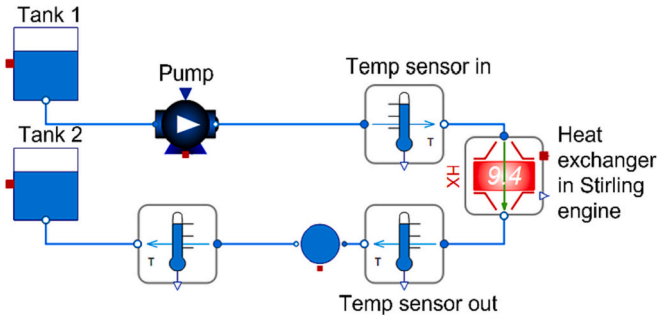

Fig. 7. Cropped view of the model showing the fluid circuit of a double tank thermal storage. Storage fluid flows from the hotter tank (no. 1), passes the Stirling engine's heat exchanger and settles in tank no. 2. The capacity of the storage is the product of the tank volume, the temperature drop over the heat exchanger and the volumetric specific heat of the fluid: $V{\cdot}dT{\cdot}c_{p,vol}$. Note the Stirling engine and cold side equipment are omitted for clarity.

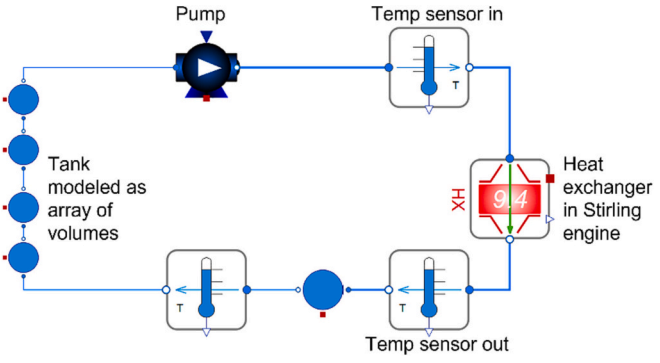

Fig. 8. Cropped view of the model showing a single tank thermal storage (tank array on the far left, here shown with four volumes for illustration purposes). Storage fluid is circulated through the tank during charge or discharge and its average temperature slowly increases or decreases. The capacity of the storage is the product of the tank volume, the temperature drop in the tank over the complete discharge phase and the volumetric specific heat of the fluid: $V{\cdot}dT{\cdot}c_{p,vol}$. Note the Stirling engine and cold side equipment are omitted for clarity.

expand the working fluid after the hot storage is charged (at cycle point no. 3 in Fig. 3). They are less often used in CB systems where the ambient is commonly used as the heat sink.

Nonetheless, a system with a cold storage in a single tank setup is modeled. In the model the heat flows to and from the hot storage during the charge and discharge phases are balanced so the hot storage returns to its initial conditions after a full cycle. It is observed that an imbalance in the cold storage prevents the cold storage returning to its initial conditions already after one or two cycles. At most combinations of T_H and T_L, the Stirling engine adds more heat to the cold storage during discharge than it draws during charge, causing the cold storage temperature to increase for each cycle. This is possibly an effect of using a single device for charge and discharge. Having different devices for charge and discharge might allow more design flexibility to balance the cold heat flows but goes against the aim of this work in addition to increasing the capital cost for the system.

The alternative to a cold storage is to use an external heat sink (during discharge) and source (during charge). The most readily available such thermal reservoir is the surrounding environment. Heat exchanging with the environment removes the need to balance the heat flows on the cold side while it has the added benefit of a simpler system. Instead of the cold storage an air-to-liquid heat exchanger (radiator) and fan are used to keep the Stirling engine's cold heat exchanger as close to the ambient temperature as possible. Costs for the cold storage are avoided, but a smaller cost for the radiator and fan are added.

Initial studies show PTES systems with a lower temperature hot side to benefit more from improved cooling than if the hot side is of high temperature. Heat transfer fluids with limited maximum temperature, i.e. synthetic oil, gain more from improved cooling than e.g. a system using Sodium for heat transport.

In light of the above, it is decided to heat exchange with the environment in this study. The radiator used here is 800 mm high, 700 mm wide and 50 mm thick. It has 144 finned tubes for cooling fluid and fin-to-fin pitch of approximately 2.0 mm. The fan has a diameter of 630 mm and delivers 7500 m^3/h at 105 Pa of pressure difference.

4. Results and discussion

The system discussed and decided upon in the previous sections is evaluated using the methodologies outlined in Section 2. Different system configurations are analyzed. First, the systems are run in discharge and charge modes in isolation in steady-state conditions to obtain representative numbers for heat flows, shaft work and electric power output.

Second, each configuration is run over two full discharge-charge cycles to obtain good estimates of round-trip efficiency. Here the operating points of the engine are balanced so that the storage returns to its starting temperature after each cycle. Ideally, there is a control system that controls power discharge and charge power according to power demand (discharging) or availability (charging) while also monitoring the storage temperature, modulating the operating point to ensure the storage returns to its desired state after each cycle. In the present work, however, the operating points for discharge and charge are selected manually.

4.1. At nominal conditions

A steady-state model is created with the hot end at constant temperature, the maximum allowed for each fluid, and a constant cold end temperature of 45°C, representative of a day with 25°C outside temperature. The Stirling engine is simulated at its highest discharge power operating point and an operating point with higher efficiency, found through exploration of the operational envelope. For the charge phase the same operating point as for the discharge is applied. It is interesting to note that for maximum power the same engine settings apply for all heat transfer fluids, meaning the lower maximum temperature of synthetic oil provides enough power to overcome fluid friction also at higher operating frequencies and pressures. In addition, note the swept volume for molten salt at the high efficiency point. There was for molten salt no increase in efficiency when decreasing the swept volume to 254 cm^3, unlike for Sodium or synthetic oil, and the higher volume used for maximum power was kept for high efficiency operation.

The use of maximum temperatures at the hot end during these steady-state simulations means the efficiency for the discharge case will be the maximum delivered during a cycle, at the beginning of the discharge phase, and the coefficient of performance for the charge case will be the minimum. Results are shown in Tables 5 and 6.

As is the case with all heat engines, efficiency is higher when the source temperature is higher. Differences in power and efficiency between the two high temperature fluids and the lower temperature fluid are evident. The thermal efficiency for synthetic oil (Omnisol) is at best 70% of the efficiency when using Sodium, decreasing to 60% at maximum power. It remains to be seen if the increase in COP with the lower sink temperature can compensate for the lower efficiency.

Efficiency increases from the maximum power point to the higher efficiency point are noteworthy, 5–7%-units, but come at the price of lower output power. Generator power is some 30–50% lower at the high efficiency operating point. The lower power output does, however, diminish the gain in net efficiency somewhat since most auxiliary power losses are independent of operating point.

With the engine in charge mode, the temperature of the hot end, now the sink, continues to influence performance. COP is highest when this temperature is 400°C, some 12% higher than when it is 600°C, but the performance of the Stirling unit as heat pump is less influenced by the hot end temperature than as heat engine. It is worth noting for the heat pump action the point of highest power is different from when operating as a heat engine. For the two higher temperature fluids the maximum heat flow occurs at 90° phase angle, where a higher COP is also seen, but for the heat engine this occurs at (-)105°. For the lower temperature HTF, Omnisol, a significant decrease in power from the point of maximum heat flow is found at the point of highest COP: 67.9 kW vs. 16.4 kW in sink heat flow, and 1.35 vs. 1.40 in $COP_{generator}$.

Performance at low temperature, such as the end of discharge or beginning of charge, are of interest. The minimum sink temperatures are estimated from fluid density and specific heat for a given storage capacity, which is the same for all fluids. The minimum cycle temperature is applied at the hot end and the results are tabulated in Tables 7 and 8. At low temperature, high efficiency operation significantly increases the performance compared to operation at maximum power but comes at the expense of a considerable decrease in power. Note COP is above 1.5 for synthetic oil and the high efficiency operating point.

A PTES system will always be run over a discharge-charge cycle. It might not return to the exact beginning state after every cycle, but more or less so, and after longer periods of operation its operation can be averaged to obtain representative periodic cycles. The performance over a complete cycle is the most relevant metric from an energy storage perspective. Table 9 shows a first glimpse of the round-trip efficiency using steady-state values for efficiency and coefficient of performance according to Eq. (19) with the hot end temperature at its maximum permissible for each fluid. The table contains two sets of data: one for maximum power and one for high performance. Details for each operating point are found in Tables 5 and 6.

With higher maximum temperatures, the round-trip efficiencies after electrical and auxiliary losses, RTE_{net}, are 40%, in some cases well over. The difference between molten nitrate salt (MS600) and Sodium is small and the choice of either will be down to economics and other considerations, such as the need for heat tracing with molten salt or special design solutions needed to prevent Sodium leakages.

The net RTE for synthetic oil is lower, between 0.27 and 0.35, but still impressively high considering the low maximum temperature. Despite the lower RTE its application could nonetheless be of interest due to the simpler, i.e. less costly, materials required with maximum

Table 5
Steady-state inputs and results for system discharge at maximum cycle temperature. Temperatures are average temperatures over the Stirling engine heat exchangers. Heat flow is from storage into Stirling engine. Efficiencies are calculated from work or power output and heat flow from storage to engine.

	MS600	Sodium	Omnisol	MS600	Sodium	Omnisol	
Operation	Max. power	Max. power	Max. power	High perf.	High perf.	High perf.	–
$p_{working}$	150	150	150	150	150	150	bar
f	25	25	25	15	15	15	Hz
V_{swept}	290	290	290	290	254	254	cm^3
ϕ_{phase}	−105	−105	−105	−120	−120	−120	°
T_{source}	550	600	400	550	600	400	°C
T_{sink}	45	45	45	45	45	45	°C
P_{aux}	800	800	800	800	800	800	W
Q_{hot}	57.1	59.2	50.4	33.1	26.6	22.5	kW
$W_{thermal}$	21.9	24.7	12.9	14.8	12.7	7.9	kW
$\eta_{thermal}$	0.38	0.42	0.26	0.45	0.48	0.35	–
η_{shaft}	0.37	0.40	0.24	0.43	0.46	0.33	–
$\eta_{generator}$	0.35	0.38	0.23	0.41	0.44	0.31	–
η_{net}	0.34	0.37	0.21	0.39	0.41	0.28	–

Table 6
Steady-state inputs and results for system charge at maximum cycle temperature. Temperatures are average temperatures over the Stirling engine heat exchangers. Heat flow is from Stirling engine into storage. Coefficients of performance are calculated from work or power input and heat flow from engine to storage.

	MS600	Sodium	Omnisol	MS600	Sodium	Omnisol	
Operation	Max. power	Max. power	Max. power	High perf.	High perf.	High perf.	–
$p_{working}$	150	150	150	150	150	150	bar
f	25	25	25	25	25	15	Hz
V_{swept}	290	290	290	290	290	218	cm^3
ϕ_{phase}	105	105	105	90	90	120	°
T_{sink}	550	600	400	550	600	400	°C
T_{source}	45	45	45	45	45	45	°C
P_{aux}	800	800	800	800	800	800	W
Q_{hot}	−64.6	−65.8	−67.9	−72.0	−73.2	−16.4	kW
$W_{thermal}$	−51.5	−53.8	−49.3	−57.0	−59.4	−11.2	kW
COP_{shaft}	1.26	1.22	1.38	1.26	1.23	1.46	–
$COP_{generator}$	1.24	1.21	1.35	1.25	1.22	1.40	–
COP_{net}	1.17	1.15	1.29	1.18	1.16	1.33	–

Table 7
Steady-state inputs and results for system discharge at minimum cycle temperature. Temperatures are average temperatures over the Stirling engine heat exchangers. Heat flow is from storage into Stirling engine. Efficiencies are calculated from work or power output and heat flow from storage to engine.

	MS600	Sodium	Omnisol	MS600	Sodium	Omnisol	
Operation	Max. power	Max. power	Max. power	High perf.	High perf.	High perf.	–
$p_{working}$	150	150	150	150	150	150	bar
f	25	25	25	15	15	15	Hz
V_{swept}	290	290	290	254	218	254	cm^3
ϕ_{phase}	−105	−105	−105	−120	−120	−120	°
T_{source}	550	600	400	550	600	400	°C
T_{sink}	45	45	45	45	45	45	°C
P_{aux}	800	800	800	800	800	800	W
Q_{hot}	52.7	53.6	45.6	23.6	18.0	20.1	kW
$W_{thermal}$	16.0	17.3	6.2	9.3	7.5	4.9	kW
$\eta_{thermal}$	0.30	0.32	0.14	0.39	0.42	0.24	–
η_{shaft}	0.29	0.31	0.12	0.37	0.39	0.22	–
$\eta_{generator}$	0.28	0.29	0.11	0.35	0.37	0.21	–
η_{net}	0.26	0.28	0.10	0.32	0.33	0.17	–

temperatures of only 400°C. Note the viscosity of synthetic oil is lower than molten salt, requiring less auxiliary pumping power. This is excluded in the present analysis.

Round trip efficiencies for low hot end temperatures are presented in Table 10. These are lower than when the maximum temperature is applied but the differences between the different fluids are less, due to the smaller difference in sink temperature at the lower end.

The round-trip efficiency of Omnisol at 300°C and maximum power is low; it is clear the high COP of 1.36 does not compensate for the low discharge efficiency. Operating at maximum power with Omnisol and the storage at its lowest temperature does not appear particularly worthwhile. Better then to operate at settings with higher round-trip efficiency and lower power, obtaining an RTE_{net} of 0.24. Note the low power has considerable effect on the net efficiency; the generator/motor round-trip efficiency is much higher at 0.32. Looking instead at operation with Sodium much higher RTE's are obtained: net values of 0.32 and 0.39 at maximum power and high efficiency operation respectively. Values at the generator/motor are again significantly higher, at 0.34 and 0.45. Again, operating at lower power yields in noticeably higher round-trip efficiencies. The situation with molten salt is similar to that with Sodium.

The performance over a cycle will contain operation at both high and

Table 8
Steady-state inputs and results for system charge at minimum cycle temperature. Temperatures are average temperatures over the Stirling engine heat exchangers. Heat flow is from Stirling engine into storage. Coefficients of performance are calculated from work or power input and heat flow from engine to storage.

	MS600	Sodium	Omnisol	MS600	Sodium	Omnisol	
Operation	Max. power	Max. power	Max. power	High perf.	High perf.	High perf.	–
$p_{working}$	150	150	150	150	150	150	bar
f	25	25	25	25	25	15	Hz
V_{swept}	290	290	290	290	290	218	cm^3
ϕ_{phase}	90	90	90	120	90	120	°
T_{sink}	450	470	300	450	470	300	°C
T_{source}	45	45	45	45	45	45	°C
P_{aux}	800	800	800	800	800	800	W
Q_{hot}	−69.3	−62.6	−65.0	−31.8	−69.8	−15.5	kW
W_{th}	−52.0	−47.7	−43.8	−23.3	−53.0	−9.2	kW
$COP_{thermal}$	1.33	1.32	1.48	1.36	1.32	1.69	–
COP_{shaft}	1.31	1.30	1.46	1.34	1.30	1.61	–
$COP_{generator}$	1.25	1.23	1.38	1.27	1.23	1.53	–
COP_{net}	1.23	1.22	1.36	1.23	1.22	1.42	–

Table 9
Steady-state round-trip efficiencies. The hot end temperature is here constant and the maximum permitted for each heat transfer fluid. The efficiency used here is thus the maximum delivered during a cycle, at the beginning of the discharge phase, and the coefficient of performance representing charge is the minimum experienced, at the end of charge.

	MS600	Sodium	Omnisol	MS600	Sodium	Omnisol	
Operation	Max. power	Max. power	Max. power	High perf.	High perf.	High perf.	–
T_{hot}	550	600	400	550	600	400	°C
RTE_{th}	0.49	0.51	0.35	0.57	0.59	0.51	–
RTE_{shaft}	0.46	0.49	0.33	0.54	0.56	0.46	–
$RTE_{generator}$	0.42	0.44	0.29	0.49	0.50	0.42	–
RTE_{net}	0.39	0.42	0.27	0.45	0.46	0.35	–

Table 10
Steady-state round-trip efficiencies. The hot end temperature is here constant and the minimum encountered for each heat transfer fluid. The efficiency used here is thus the maximum delivered during a cycle, at the beginning of the discharge phase, and the coefficient of performance representing charge is the minimum experienced, at the end of charge.

	MS600	Sodium	Omnisol	MS600	Sodium	Omnisol	
Operation	Max. power	Max. power	Max. power	High perf.	High perf.	High perf.	–
T_{hot}	450	470	300	450	470	300	°C
RTE_{th}	0.41	0.42	0.20	0.54	0.55	0.41	–
RTE_{shaft}	0.38	0.40	0.17	0.50	0.51	0.36	–
$RTE_{generator}$	0.34	0.36	0.16	0.45	0.46	0.32	–
RTE_{net}	0.32	0.34	0.13	0.39	0.40	0.24	–

low storage temperatures and as a final note on the steady-state operation a table of average round-trip efficiencies is assembled, Table 11.

When using Sodium net round-trip efficiencies between 0.38 and 0.43 result and at the generator/motor they are between 0.40 and 0.43. For synthetic oil they are net between 0.20 and 0.29, while at generator/motor they are between 0.23 and 0.37. Molten salt performs similarly to Sodium.

It is clear that accounting for the varying inlet temperatures to the Stirling engine is important. A system needs to be run over a full cycle with the hot storage included to obtain an accurate temperature profile over time. In addition, when a system is cycled there needs to be thermal balance between the discharge and charge for the system to return to its initial condition after each cycle. The energy output during discharge needs to be the same as the energy input during charge. Different operating points might thus be needed for discharge and charge. This is looked at in the next section.

4.2. Over a cycle

When PTES systems are operated over a complete cycle the inlet temperature into the Stirling engine's hot heat exchanger varies with time. Temperatures decrease during the discharge phase, decreasing

Table 11
Average steady-state round-trip efficiencies, i.e. the average of those presented in Tables 9 and 10.

	MS600	Sodium	Omnisol	MS600	Sodium	Omnisol	
Operation	Max. power	Max. power	Max. power	High perf.	High perf.	High perf.	–
T_{hot}	550/450	600/470	400/300	550/450	600/470	400/300	°C
RTE_{th}	0.45	0.47	0.28	0.55	0.57	0.46	–
RTE_{shaft}	0.42	0.45	0.25	0.52	0.53	0.41	–
$RTE_{generator}$	0.38	0.40	0.23	0.47	0.48	0.37	–
RTE_{net}	0.36	0.38	0.20	0.42	0.43	0.29	–

efficiency, while during the charge phase they increase, decreasing COP. Efficiency will thus be greatest at the beginning of discharge, and, similarly, COP will be greatest at the beginning of charge. Similarly, temperatures in the cold heat exchanger will also vary since they are dependent on the operating point of the Stirling engine and the magnitude of its residual heat output.

To obtain thermal balance between the discharge and charge phases, different operating points for each phase are needed. It turns out that more or less the same operating points are suitable for all three storage fluids. Over a full cycle time of 24 h it is decided to discharge for 14 h and charge for the remaining 10 h. This is reasonably representative of a setup where charging is done with power from a solar photovoltaic array.

Ideally, there would be a control system that decides the operating point for each phase according to an external input of discharge power demand or charge power availability. For most practical applications these would vary with time. Note there is no need to return to the exact same state after each cycle. The end state after each cycle would be a result of operation optimization, possibly using forward looking forecasting algorithms [33]. For the present work calculating round-trip efficiencies is the primary interest, and for easy calculation of the same it is necessary to return to the initial state after each cycle in order to avoid simulation over a prolonged period of time (during which many cycles could be averaged). To simplify the present study, operating points are manually selected and are chosen so that the two phases are thermally balanced.

Unless otherwise noted, analyses are run using an ambient temperature of 25°C and a hot storage tank volume of 15 m^3 for Sodium and synthetic oil. For molten salt a smaller volume of 7.5 m^3 is used due to its higher density. Auxiliary power losses are constant at 350 W and the self-consumption of the radiator fan is calculated by the model and included in the net values of round-trip efficiency and power. Storage initialization temperatures are set as the maximum permissible for each storage fluid. Fig. 9 shows inlet temperatures to the engine heat exchanger when systems are cycled twice. The differences in temperature decrease over e.g. the discharge phase due to differences in volumetric specific heat are clearly seen and they show why a smaller storage volume is sufficient when using molten salt. It also shows that with synthetic oil a larger storage might be beneficial to keep the temperature drop over the discharge phase small. Here, it approaches 300°C and with a twice as large storage volume it could be kept above 350°C. The associated increase in discharge efficiency could be useful.

Calculated round-trip efficiencies for the cycles are shown in Table 12. They are higher than those calculated for maximum power in the average round-trip in Table 11. Net RTE's are high with molten salt and Sodium, close to or over 0.40, due to their high maximum temperatures. With synthetic oil, 0.25 is reached. This is in the lower end of the previously quoted range for thermal storage systems [10] but with a much simpler concept and potentially lower cost than turbomachinery-based designs.

Table 12
Cycle round-trip efficiencies averaged over two cycles. Constant ambient conditions and auxiliary power loss. Averaged over two cycles. DF is the discharge duration as a fraction of the full cycle.

	MS600	Sodium (Na)	Omnisol	
$p_{working,\ dis}$	150	150	150	bar
$f_{discharge}$	19	19	19	Hz
$V_{swept,dis}$	290	290	290	cm^3
$\phi_{phase,dis}$	−120	−120	−120	°
$p_{working,\ ch}$	150	150	150	bar
f_{charge}	21	21	20	Hz
$V_{swept,ch}$	290	290	290	cm^3
$\phi_{phase,ch}$	105	105	105	°
V_{tank}	7.5	15	15	m^3
DF	58.333	58.333	58.333	%
$T_{storage,\ init}$	550	600	400	°C
$E_{generator}$	199	216	106	kWh
$RTE_{generator}$	0.43	0.45	0.28	–
RTE_{net}	0.40	0.43	0.25	–

The discharged energy is not the same for the three cases, despite using the same operational parameters. In addition to low round-trip efficiency, using synthetic oil as thermal fluid reduces energy output from the generator from 216 kWh with Sodium to 106 kWh, a reduction of 51%. A Stirling engine is a heat engine, and the temperature delivered to the Stirling engine affects its efficiency and power output. Now, a system can be scaled to the desired power output, so it could be argued power output is of secondary importance compared to efficiency, but one must then be aware of the cost penalty for a larger engine when comparing.

Fig. 10 shows efficiencies and COP's for two cycles. Synthetic oil has the highest COP, but also the lowest discharge efficiency. It has the lowest RTE, and it is clear that the higher COP cannot offset the lower efficiency. For the two high temperature fluids there seems to be a good balance between efficiency and COP resulting in high RTE, while not requiring superalloys in construction.

The difference in RTE between molten nitrate salt (MS600) and Sodium is small and the choice of either will be down to economics and other considerations, including the choice of storage volume, while synthetic oil could still be of interest due to the less costly materials

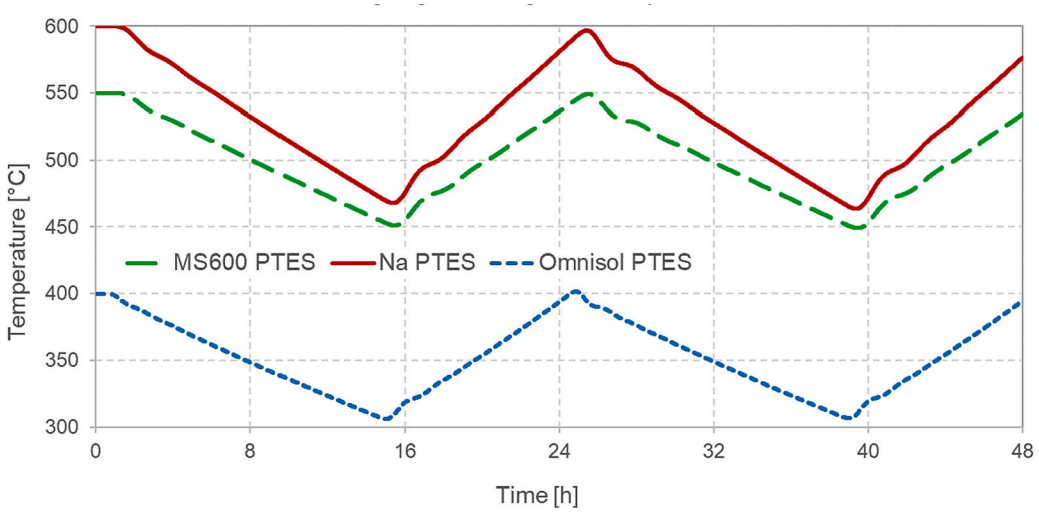

Fig. 9. The average inlet temperature to the Stirling engine over two full cycles (discharge-charge-discharge-charge).

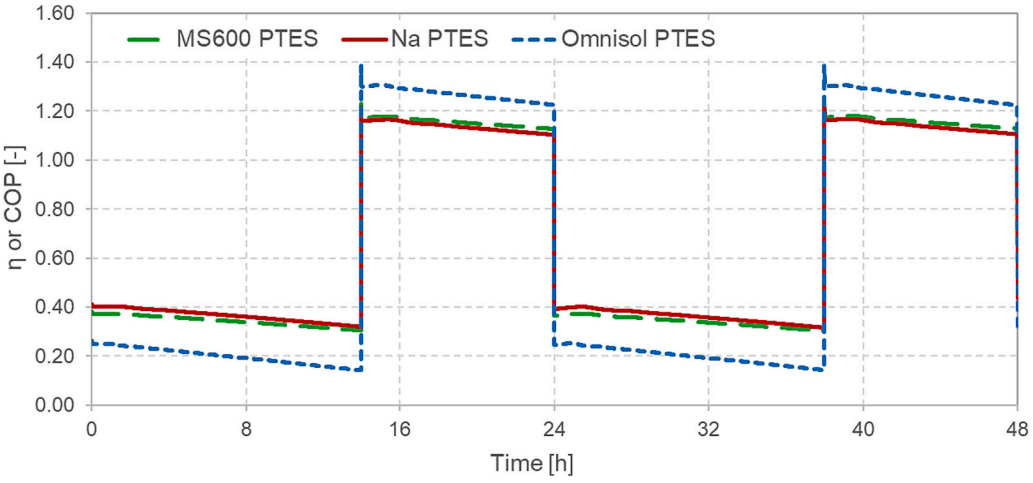

Fig. 10. Discharge efficiency and charging coefficient of performance (COP) over two full cycles (discharge-charge-discharge-charge).

required.

Sodium can manage up to 800°C, and a higher maximum storage temperature for the Sodium system is studied. A higher maximum temperature yields higher RTE, but the COP is lower and approaches unity. Close to unity the benefit of the heat pump is small and a Carnot battery might be a more economical approach at higher temperatures. In addition, more advanced materials are required beyond 600°C, due to decreased material strength and increased temperature corrosion at elevated temperatures. Appendix B shows efficiency and COP for cases with higher temperatures with Sodium.

Investigating the efficiency potential of the proposed system, the engine is modulated with the aim to increase efficiency, with less regard to power output than the previous analysis. The operating points for charge and discharge are modified to obtain highest possible round-trip efficiency while maintaining thermal balance between the phases. It is achieved through lowering of the operating frequency and changing the phase angle during charge to 90° for molten salt and Sodium. For Sodium and synthetic oil decreasing the swept volume has a positive effect. Note the increase in RTE at the generator. It is larger than the net RTE increase since the auxiliary power consumption is independent of operating point and has more impact at lower power output. Results are summarized in Table 13.

Systems with molten salt gain the least, Sodium systems gain 6%-units of RTE calculated at the generator and 4%-units of net RTE, while systems with synthetic oil gain 11% units and 7%-units respectively. Delivered energy is however lower. Over two cycles it decreases 22 and 59 kWh for molten salt and Sodium, but only 10 kWh with synthetic oil. It thus seems advantageous for systems with synthetic oil to cut back on the power for a substantial increase in round-trip efficiency.

Considering the simplicity of the system: a single piece of machinery for discharge and charge and no cold storage, a demonstrated efficiency potential of close to 50% is noteworthy. More so is the efficiency potential of almost 40% at the generator/motor for a system with a maximum temperature of a mere 400°C.

It is worth pointing out the cold end temperature during system charge. It is around 5°C lower than the surrounding environment and could potentially be valuable for e.g. building cooling in sufficiently hot climates, as long as the temperature of the inlet air to the radiator, i.e. the temperature of the heat source, remains constant. It should also be noted that the ambient temperature used here is a moderate 25°C and higher ambient temperatures will improve the COP when charging, but of course also lower the discharge efficiency. A system with Omnisol as heat transfer fluid and operating as in Table 13 will in ambient temperatures of 35°C deliver a net round-trip efficiency of 0.30, i.e. a decrease of 2%-units.

Decreasing the tank volume in the hot storage will lower the cost of the storage medium. However, it will also lower the average inlet temperature to the Stirling engine, lowering the discharge efficiency while increasing the charge COP. To which extent the performance is compromised by the smaller volumes is interesting and storage volumes of 3.3, 8.6 and 7.5 m^3 are applied to systems using molten salt, Sodium and synthetic oil, respectively. The volumes are selected to provide the same storage capacity for all three cases, namely 2.47 kWh/K. The

Table 13
Cycle round-trip efficiencies at reduced power operating points for higher round-trip efficiency averaged over two cycles. Constant ambient conditions and auxiliary power loss. DF is the discharge duration as a fraction of the full cycle.

	MS600	Sodium (Na)	Omnisol	
$p_{working,\ dis}$	150	150	150	bar
$f_{discharge}$	15	15	15	Hz
$V_{swept,dis}$	290	254	262	cm^3
$\phi_{phase,dis}$	−120	−120	−120	°
$p_{working,\ ch}$	150	142	140	bar
f_{charge}	15.5	15	15	Hz
$V_{swept,ch}$	290	272	290	cm^3
$\phi_{phase,ch}$	90	90	105	°
V_{tank}	7.5	15	15	m^3
DF	58.333	58.333	58.333	%
$T_{storage,\ init}$	550	600	400	°C
$E_{generator}$	178	157	96	kWh
$RTE_{generator}$	0.47	0.49	0.37	–
RTE_{net}	0.43	0.45	0.32	–

Table 14
Cycle round-trip efficiencies at reduced power operating points for higher round-trip efficiency and smaller tank volumes, averaged over two cycles. Constant ambient conditions and auxiliary power loss. DF is the discharge duration as a fraction of the full cycle.

	MS600	Sodium (Na)	Omnisol	
$p_{working,\ dis}$	150	150	150	bar
f_{dis}	15	15	15	Hz
$V_{swept,dis}$	290	254	268	cm^3
$\phi_{phase,dis}$	−120	−120	−120	°
$p_{working,\ ch}$	150	140	140	bar
f_{charge}	15.5	15	15	Hz
$V_{swept,ch}$	290	290	290	cm^3
$\phi_{phase,ch}$	90	105	105	°
V_{tank}	3.3	8.6	7.5	m^3
DF	58.333	58.333	58.333	%
$T_{storage,\ init}$	550	600	400	°C
$E_{generator}$	133	148	83	kWh
$RTE_{generator}$	0.45	0.47	0.33	–
RTE_{net}	0.40	0.43	0.28	–

operating points are adjusted minimally to provide thermal balance between discharge and charge. Results are shown in Table 14.

A comparison of data from Tables 13 and 14 shows the reductions in performance with smaller storage volumes to be small. If the cost of the storage media and the tank is high the optimal system could very well have a smaller tank volume than what was used as baseline here. Appendix C shows the average inlet temperature to the Stirling engine for the tank volumes in Table 14 for two fluids: molten salt and synthetic oil.

4.3. Comparison with a Carnot battery

The above analyses were made on systems where a Stirling cycle was operated in reverse, charging the thermal storage in heat pump mode. Energy as electricity or mechanical work is input to the cycle and is augmented by the heat extracted from the surrounding environment. To demonstrate the effect of using a thermodynamic cycle for charging, comparative analyses are made on a Carnot battery system employing the same Stirling engine for discharge but using a resistive electrical heater for charge. The effective coefficient of performance for the charge process is thus just below unity since the electrical heater and its associated control equipment has some power losses.

Inlet temperatures to the Stirling engine are shown in Fig. 11 for the maximum power cases. The temperatures are almost identical between the PTES and the CB systems and indicate the two systems provide the same conditions to the Stirling engine during discharge. Discharge efficiency and charging COP are shown in Fig. 12 where molten salt is used as storage fluid. The higher COP of the pumped system is evident, but for molten salt its maximum is limited to about 1.20. The advantage of the heat pump operation is more evident when the maximum hot temperature is lower, as is the case with synthetic oil, and this is visible in Fig. 13.

Round-trip efficiencies and energy outputs are summarized in Table 15. The energy outputs of the two systems are almost identical, while the round-trip efficiency is clearly higher with the pumped system. The benefit of the heat pump operation is evident.

4.4. Energy and power densities

Energy and power densities are of interest when comparing different technologies and when estimating land use. Data from the present study is used to estimate these for Stirling based PTES systems, see Table 16. Energy and power vary with maximum temperature, storage volume and operating point and the densities are calculated for each combination. The energy delivered by each system over a complete cycle is used for the energy density, and the average power delivered during system discharge over a cycle is used in the calculation of the power density. The power conversion unit, i.e. the Stirling unit, and auxiliary equipment, e.g. pumps, radiator, fan, power electronics, etc., are estimated to occupy 1.5 m^3 of volume.

Energy densities calculated for Stirling based PTES span from 6 to 28 kWh/m^3, with the high value seen with molten salt and a small storage volume. The low value is for synthetic oil and the largest storage volume simulated. The density range is similar to that quoted by [10] for CAES and in the lower end of that for Brayton PTES. Power densities are again the same as given by [10] for CAES and in the lower range to those for Brayton PTES. The high value of 2 kW/m^3 is for molten salt and a small storage volume, where the low value is for synthetic oil and a larger storage volume. If density is the most important parameter molten salt is the preferred heat transfer and storage fluid, and a small storage volume is the best option.

5. Conclusions

The main theme of the work was to investigate simpler and smaller thermal storage technologies. Conventional PTES systems typically use Brayton cycles which are complex and costly with two sets of turbomachinery. The Rankine cycle-based CHEST system offers some simplification but is commonly proposed for larger systems. There is thus a gap to be filled with a smaller and less costly and complex thermal energy storage solution.

The first investigative topic of this article was whether a Stirling based PTES system can be built with one piece of machinery acting both as heat engine and as heat pump. The answer here must be yes. It has been demonstrated that one Stirling engine can function both as heat engine, discharging heat from the storage to produce electricity via a generator, and as heat pump, utilizing available electricity and an available heat source to charge the thermal storage. The proposed configuration offers a substantial reduction in system complexity and enables a smaller minimum size of the power conversion unit than what is practical using conventionally designed pumped thermal energy storage systems based on the Brayton cycle. The proposed concept provides an alternative for applications that require less than 100 kW of discharge power.

The second topic related to suitable types of storage and which heat transfer fluid to use, and the need for storage on the cold side. Analysis showed thermal energy storage only on the hot side to be sufficient, and that heat exchanging with the environment on the cold side is favorable over a cold side storage. The present work showed single-tank liquid hot

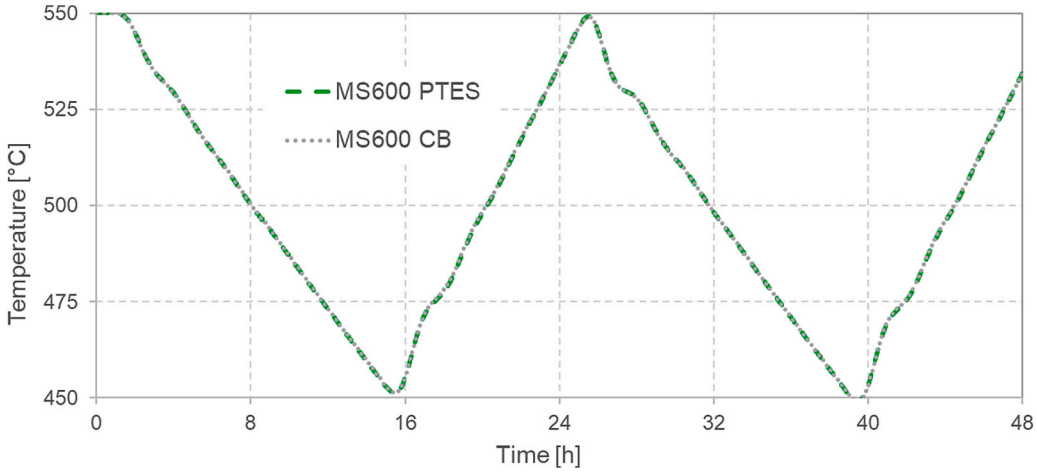

Fig. 11. The average inlet temperatures to the Stirling engine over two full cycles (discharge-charge-discharge-charge) for a PTES system and a CB system, both with molten salt as storage material and heat transfer fluid. Note the temperatures are almost identical, indicating the two systems provide the same conditions to the Stirling engine during discharge.

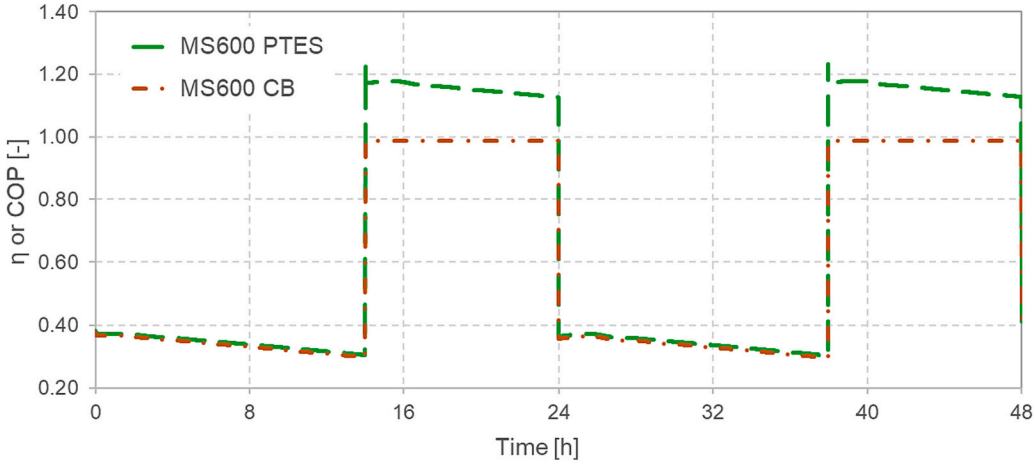

Fig. 12. Discharge efficiency and charging coefficient of performance (COP) over two full cycles (discharge-charge-discharge-charge) for a PTES system and a CB system, both with molten salt as storage material and heat transfer fluid.

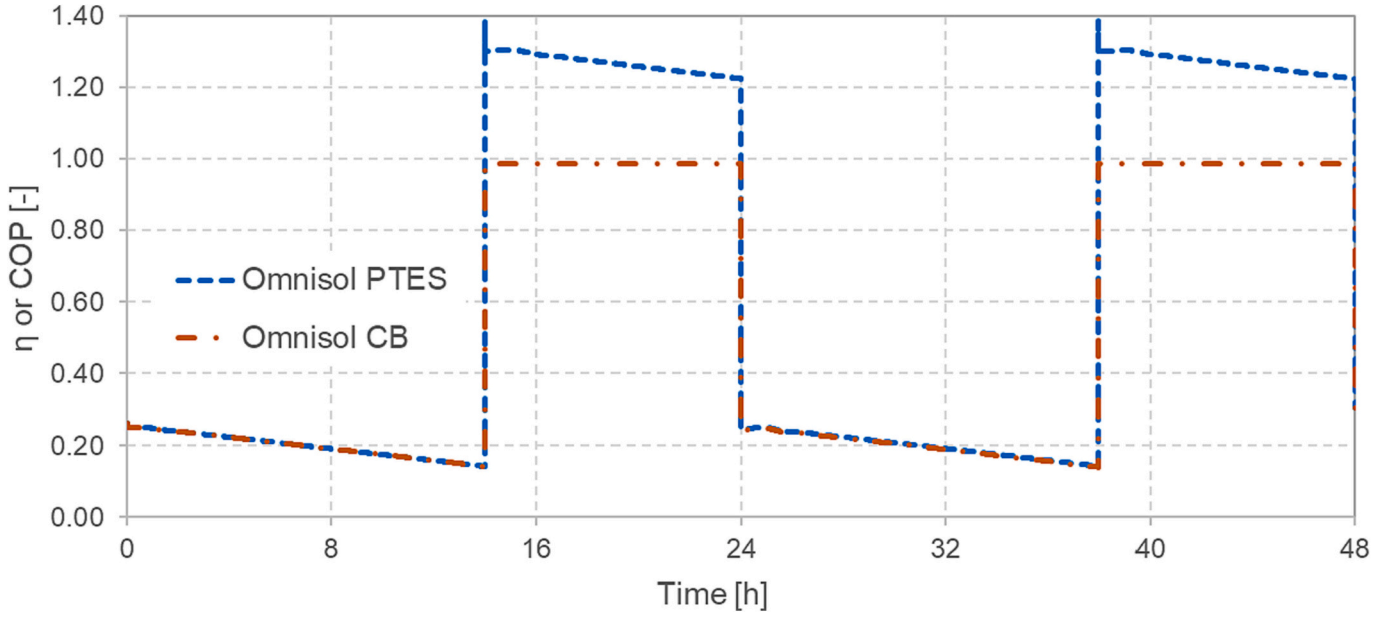

Fig. 13. Discharge efficiency and charging coefficient of performance (COP) over two full cycles (discharge-charge-discharge-charge) for a PTES system and a CB system, both with synthetic oil as storage material and heat transfer fluid.

storages to be preferred over dual-tank storages when paired with Stirling engines. In addition, during system charge it is possible to make use of the residual cold air or coolant from the cold side. Regarding storage medium, any of the three fluids included in the study have been shown to work well from their respective characteristics. The choice of either is down to the requirements of a specific system.

The third task was to calculate representative flows of energy and mass, temperature levels, and make estimates of discharge efficiency, COP, and round-trip efficiency. For the chosen system size, values are obtained for heat flow, power, and temperature levels using models where the core components have previously been validated against experimental data. Round-trip efficiencies up to 49% at the generator are calculated for high-temperature fluids and around 32 % for low-temperature synthetic fluids. Energy densities of 6–28 kWh/m^3 and 0.5–2 kW/m^3 are estimated.

The final task was to make a comparison with a Carnot Battery with direct electrical heating of the hot storage. It clearly showed the benefit of the heat pump in the charging phase.

In summary, the present work has shown a Stirling based PTES with a sensible liquid thermal storage on the hot side only to have competitive round-trip efficiency and system densities when compared to other thermo-mechanical energy storage systems.

5.1. *Summary of the conclusions*

The conclusions are summarized as follows.

- A Stirling based pumped thermal energy storage with a single Stirling machine can perform both the heat pump function and act as a heat engine to produce electricity via a generator.
- Having a thermal energy storage only on the hot side is sufficient and heat exchanging with the environment on the cold side is favorable over a cold side storage.
- A single-tank liquid hot storage is preferred over dual-tank storages when paired with Stirling engines.
- Any of the three types of heat transfer fluids work well from their respective characteristics.

Table 15
Cycle round-trip efficiencies at constant ambient conditions and auxiliary power loss for a pumped thermal storage system and a Carnot battery with electrical charging. DF is the discharge duration as a fraction of the full cycle.

	PTES with MS600	PTES with Omnisol	CB with MS600	CB with Omnisol	
$p_{working,\ dis}$	150	150	150	150	bar
$f_{discharge}$	19	19	15	19	Hz
$V_{swept,dis}$	290	290	290	290	cm^3
$\phi_{phase,dis}$	−120	−120	−120	−120	°
$p_{working,\ ch}$	150	150	–	–	bar
f_{charge}	21	20	–	–	Hz
$V_{swept,ch}$	290	290	–	–	cm^3
$\phi_{phase,ch}$	105	105	–	–	°
P_{charge}	–	–	55	48	kW
V_{tank}	7.5	15	7.5	15	m^3
DF	58.333	58.333	58.333	58.333	%
$T_{storage,\ init}$	550	400	550	400	°C
$E_{generator}$	199	106	195	105	kWh
$RTE_{generator}$	0.43	0.28	0.36	0.22	–
RTE_{net}	0.40	0.25	0.34	0.20	–

Table 16
Energy and power densities, ρ_E and ρ_P. Values for CAES, Brayton PTES and CHEST are collected from [10]. Values for Stirling PTES are calculated using data from the present study.

	ρ_E	ρ_P
	kWh/m^3	kW/m^3
CAES	3–20	0.5–2
Brayton PTES	20–50	1–15
CHEST	40–100	0.5–17
Stirling PTES	6–28	0.5–2

- Simulations show the proposed concept to have high round-trip efficiency, comparable to conventional pumped thermal energy storage systems. The round-trip efficiency potential is close to 50% with high temperature fluids and above 30% with a temperature limit of 400°C.

CRediT authorship contribution statement

All work in the present paper is original work by the (only) author, i.e. Martin Nilsson.

Declaration of competing interest

The authors declare the following financial interests/personal relationships which may be considered as potential competing interests: Martin Nilsson reports a previous relationship with Azelio AB that includes: employment and equity or stocks. Martin Nilsson has patent pending to Azelio AB.

Data availability

The authors do not have permission to share data.

Acknowledgements

The author thanks Ty Nieses at the National Renewable Energy Laboratory in the United States of America for inspiration and valuable discussions. His inquisitive curiousness inspired the author to the formulation of the central concept of this work.

Appendix A

Coefficients for meta-model functions f_1, f_2 and f_3 for engine discharge.

Coefficient	f_1	f_2	f_3
C_0	20,712	−11,846	8084
C_1	3163	1288	3647
C_2	−685	−124	−925
C_3	12,685	−8512	4221
C_4	913	−652	216
C_5	5089	−3584	1425
C_6	4150	−2714	1396
C_7	2874	−2365	544
C_8	2403	−1697	664
C_9	1799	740	2557
C_{10}	572	−438	−561
C_{11}	−397	−147	214
C_{12}	928	−738	1074
C_{13}	781	359	811
C_{14}	613	173	525
C_{15}	254	−154	705
C_{16}	178	−135	−202
C_{17}	520	−474	110
C_{18}	412	135	−125
C_{19}	460	212	−213
C_{20}	102	−98	−171
C_{21}	149	−111	−499
C_{22}	−89	−113	219
C_{23}	−31	−14	137
C_{24}	1730	−1635	214
C_{25}	−81	−48	−307

(*continued on next page*)

(*continued*)

Coefficient	f_1	f_2	f_3
C_{26}	−62	−33	486
C_{27}	−160	−41	8084
C_{28}	−138	−31	3647
C_{29}	−369	−139	
C_{30}	141	60	
C_{31}	87	58	
C_{32}	131	108	

Appendix B

Discharge efficiency and charging coefficient of performance (COP) over two full cycles (discharge-charge-discharge-charge) for the baseline maximum temperature of 600°C and two higher temperatures, 700°C and 800°C.

Note the COP is just above unity for the 800°C case at the end of charge, indicating only a small benefit from the heat pump action. Also note the substantially increased discharge efficiency at higher temperatures.

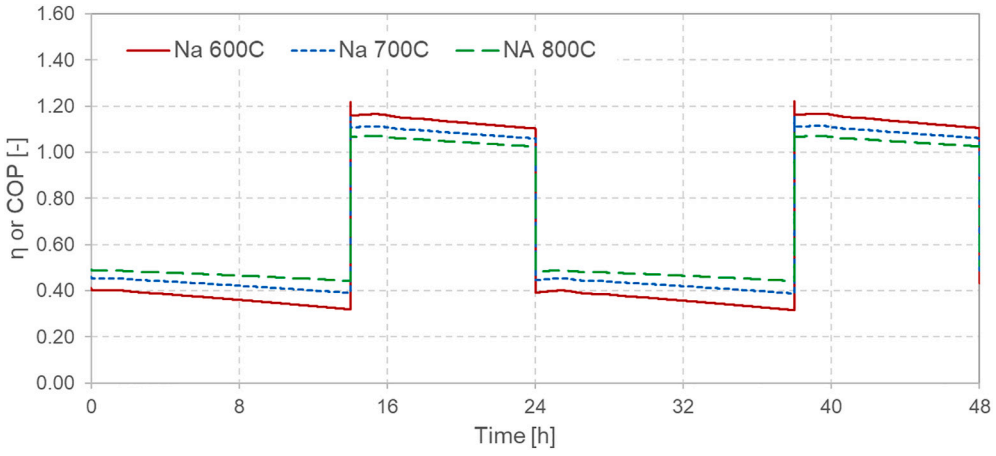

Appendix C

The average inlet temperature to the Stirling engine over two full cycles (discharge-charge-discharge-charge) for molten salt (MS600) and two tank volumes is shown below. The baseline tank volume of 7.5 m^3 is accompanied by data for a 3.3 m^3 tank. The lower minimum temperature with the smaller tank is clearly visible. The 56% reduction in volume results in a circa 75°C lower minimum temperature.

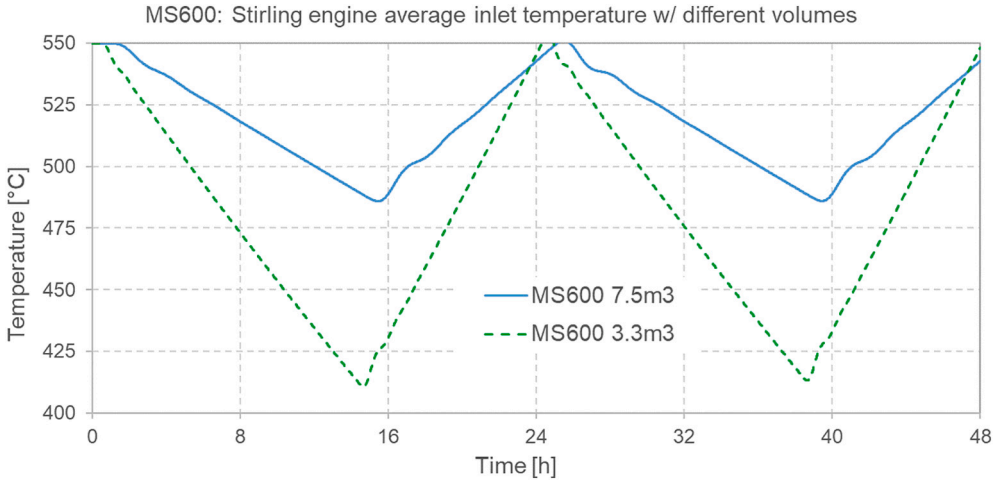

The average inlet temperature to the Stirling engine over two full cycles (discharge-charge-discharge-charge) for synthetic oil (Omnisol) is shown below. The baseline tank volume of 15 m^3 is accompanied by data for a 7.5 m^3 tank. The lower minimum temperature with the smaller tank is clearly visible. The 50% reduction in volume results in a circa 50°C lower minimum temperature.

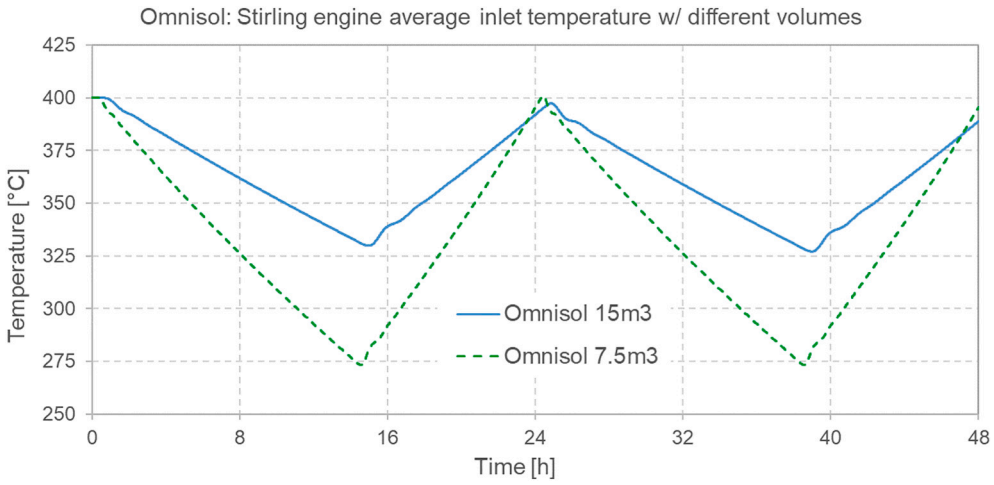

References

[1] Europe's rivers run dry as scientists warn drought could be worst in 500 years. Article. The Guardian. On-line edition. Retrieved 2022-08-14.
[2] US issues western water cuts as drought leaves Colorado River near 'tipping point.' Article. The Guardian. On-line edition. Retrieved 2022-08-21.
[3] China drought causes Yangtze to dry up, sparking shortage of hydropower. Article. The Guardian. On-line edition. Retrieved 2022-08-22.
[4] World Energy Outlook. Report. Paris: International Energy Agency, 2021.
[5] Net-zero power. Long duration energy storage for a renewable grid. Report. Long Duration Energy Storage Council, 2021.
[6] House C, Way N. The world's water battery: pumped hydropower storage and the clean energy transition. International Hydropower Association. n.d.
[7] A. Vecchi, et al., Liquid air energy storage (LAES): a review on technology state-of-the-art, integration pathways and future perspectives, Adv. Appl. Energy (2021), https://doi.org/10.1016/j.adapen.2021.100047.
[8] V. Novotny, Review of Carnot battery technology commercial development, Energies 15 (2) (2022) 647, https://doi.org/10.3390/en15020647.
[9] O. Dumont, G.F. Frate, A. Pillai, S. Lecompte, M. De Paepe, V. Lemort, Carnot battery technology: a state-of-the-art review, J. Energy Storage 32 (2020) 101756.
[10] A. Olympios, J. McTigue, P. Farres-Antunez, A. Romagnoli, W. Steinmann, A. Thess, L. Wang, H. Chen, Y. Li, Y. Ding, C.N. Markides, Progress and prospects of thermo-mechanical energy storage - a critical review, IOP Progress in Energy 3. doi:https://doi.org/10.1088/2516-1083/abdbba.
[11] T. Lindquist, A novel modular and dispatchable CSP Stirling system: design, validation, and demonstration plans, AIP Conf. Proc. 2126 (2019), 060005, https://doi.org/10.1063/1.5117591.
[12] M. Nilsson, A. Abou-Taouk, H. Sandberg, J. Lindh, A Stirling engine for thermal energy storage, AIP Conf. Proc. 2126 (2019) 140005, https://doi.org/10.1063/1.5117653.
[13] G. Glatzmeier, Solar thermoelectricity via advanced latent heat storage: a cost-effective small-scale CSP application, AIP Conf. Proc. 030019 (1850) 2017, https://doi.org/10.1063/1.4984362.
[14] J. Rea, Prototype latent heat storage system with aluminum-silicon as a phase change material and a Stirling engine for electricity generation, Energ. Conver. Manage. (2019), https://doi.org/10.1016/j.enconman.2019.111992.
[15] S. Tetteh, M.R. Yazdani, A. Santasalo-Aarnio, Cost-effective Electro-Thermal Energy Storage to balance small scale renewable energy systems, J. Energy Storage (2021), https://doi.org/10.1016/j.est.2021.
[16] W.D. Steinmann, The CHEST (Compressed Heat Energy STorage) concept for facility scale thermo mechanical energy storage, Energy 69 (2014) 543–552, https://doi.org/10.1016/j.energy.2014.03.049.
[17] T. Desrues, A thermal energy storage process for large scale electric applications, in: Applied Thermal Engineering, 2009, https://doi.org/10.1016/j.applthermaleng.2009.10.002.
[18] R.B. Laughlin, Pumped thermal grid storage with heat exchange, J. Renew. Sustain. Energy (2017), https://doi.org/10.1063/1.4994054.
[19] J. McTigue, et al., Techno-economic analysis of recuperated Joule-Brayton pumped thermal energy storage, in: Energy Conversion and Management, 2021, https://doi.org/10.1016/j.enconman.2021.115016.
[20] P. Tafur-Escanta, Electrical energy storage using a supercritical CO2 heat pump, in: The 8th International Conference on Energy and Environment Research ICEER 2021, 13–17 September, 2021, https://doi.org/10.1016/j.egyr.2022.01.073.
[21] J. Howes, Concept and Development of a Pumped Heat Electricity Storage Device. Proceedings of the IEEE Vol. 100, No. 2, 2012.
[22] P. Fritzson, Principles of Object-Oriented Modeling and Simulation with Modelica 3.3, John Wiley & Sons, New York, 2014 (ISBN 9781-118-859124).
[23] N. Andersson, L.-E. Eriksson, M. Nilsson, Numerical Simulation of Stirling Engines Using an Unsteady Quasi-One-Dimensional Approach, Journal of Fluids Engineering - Transactions of The ASME (0098-2202) Vol. 137, 2015 ((2015), 5, p. Art. no. 051104).
[24] M. Nilsson, P. Wåhlen, A. Mattsson, Performance Testing of a Stirling Engine, With Implementation of High-Speed Pressure Measurements in the Working Gas Channel, 16th International Stirling Engine Conference, Sept. 24-26, 2014, Bilbao, Spain, 2014.
[25] Datasheet W3G630, EBM Papst, https://ebmpapst.se/sv/dat/media_manager/pid/2526/product-documents/W3G630DU2302.pdf, retrieved on 2023-08-21.
[26] M. Condé, Thermophysical Properties of Brines. Report. M. Condé Engineering. Zürich, 2011.
[27] J.K. Fink and L. Leibowitz. Thermodynamic and Transport Properties of Sodium Liquid and Vapor. Report. Argonne National Laboratory. ANL-/RE-95/2.
[28] M. Nilsson, "On Stirling Engine Thermodynamic Modeling", Thesis for the Degree of Licenciate of Technology, ISSN 1652–8565, Chalmers University of Technology, Gothenburg, Sweden, 2016.
[29] A. Organ, The Regenerator and the Stirling Engine, Mechanical Engineering Publications, London, 1997.
[30] C.M. Hargreaves, The Philips Stirling Engine, Elsevier, 1991.
[31] G. Lundholm, The Experimental V4X Stirling Engine – A Pioneering Development, Internal Report, Lund University, Department of Heat and Power Engineering, 1999.
[32] A. Baumüller, G. Lundholm, L. Lundström, W. Schiel, Development History of the V160 and SOLO Stirling 161 Engines, 9th ISEC, Pilanesburg, South Africa, 2–4, June 1999.
[33] K. Antoniadou-Plytaria, et al., Effect of Short-Term and High-Resolution Load Forecasting Errors on Microgrid Operation Costs, 2022 IEEE PES Innovative Smart Grid Technologies Conference Europe (ISGT-Europe), Novi Sad, Serbia, 2022, pp. 1–5, https://doi.org/10.1109/ISGT-Europe54678.2022.9960535.